Quantum Theory for the Computer Age

Unit 8

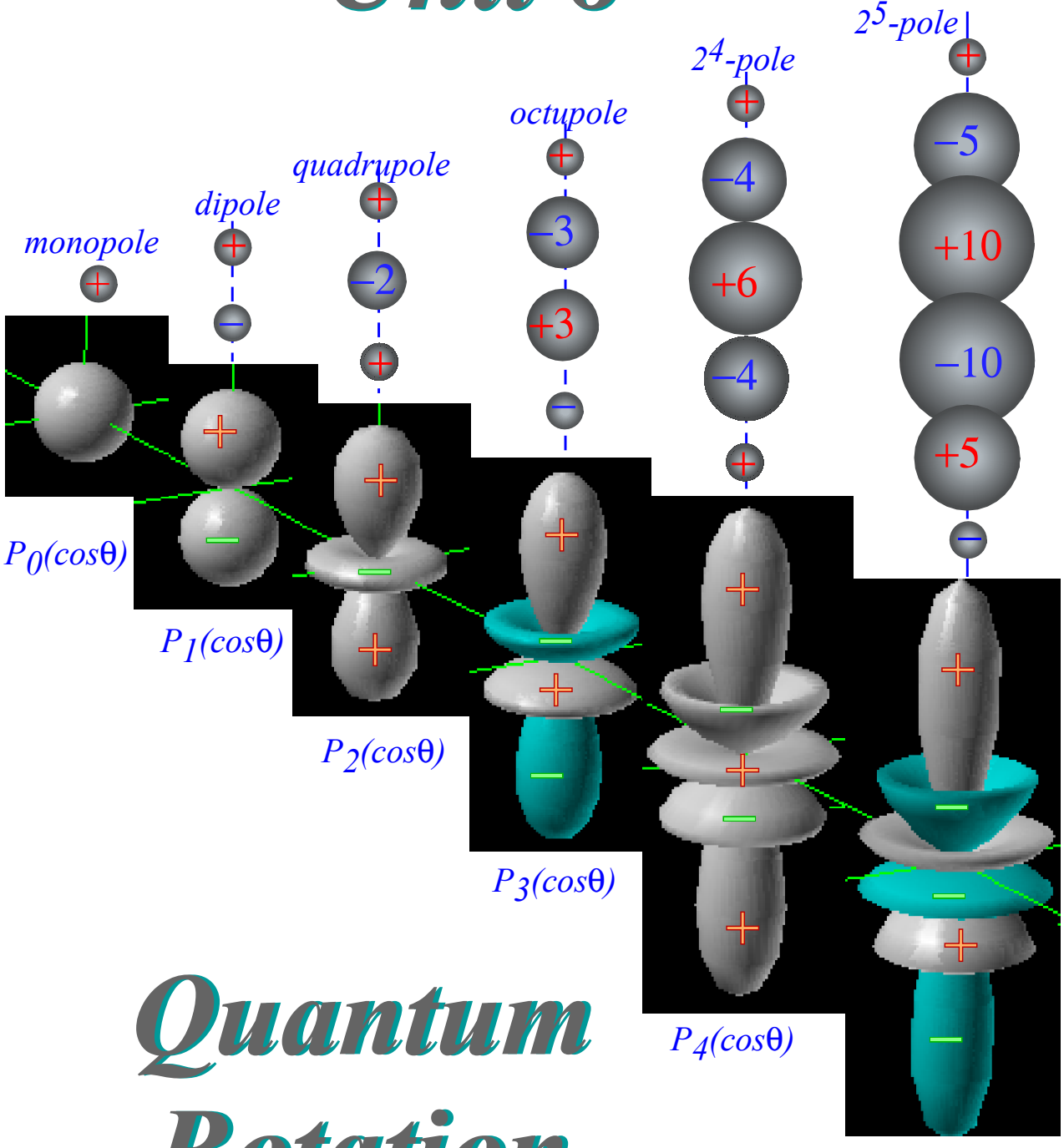

Quantum Rotation

Unit 8 Quantum Rotation

Quantum theory of rotation and angular momentum is described in terms of quantum oscillation using a synthesis of ideas developed by Hamilton, Stokes, Schwinger, and Feynman. In the present Unit 8 the theory of quantum 2D oscillator from Unit 7 is used to derive 3D quantum rotational states, operators, and their representations. The ABCD model of coupled oscillators and 2-state or U(2) spin-1/2 analogies of Unit. 3 Chapter 10 is also part of the development as is the non-Abelian symmetry theory of Chapter 15. This unit is a step in the development of Wigner-Racah quantum theory of angular momentum that is the foundation of modern atomic, molecular, optical, and nuclear physics.

W. G. Harter

Department of Physics

University of Arkansas

Fayetteville

Hardware and Software by

HARTER-*Soft*

Elegant Educational Tools Since 2001

Unit 8 Quantum Rotation

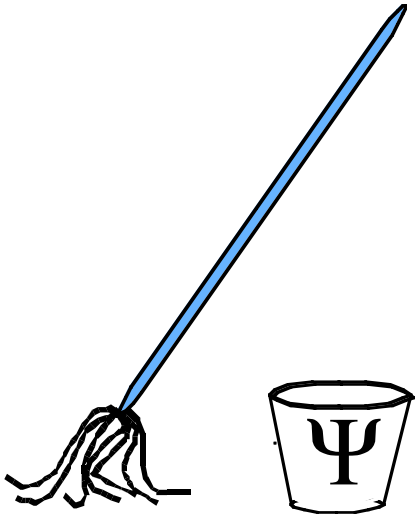

QM for AMOP

Chapter 23

Spin and Rotation Operators, States, and Dynamics

W. G. Harter

Using the 2D-harmonic oscillator algebra from the earlier Chapter 21, the quantum mechanics of 3D rotation and angular momentum states are developed. By using the ABCD oscillator 2-state system analogy of Chapter 10 we extend the development, due to Schwinger, of the quantum theory of angular momentum to include that of an entire body (nucleus, molecule, cluster, etc.) not just a single point particle. The idea of dual sets of quantum operators, internal (body) as well as external (lab) operators, was introduced in Chapter 15 and is developed again here to make convenient and powerful tools for visualization as well as computation of quantum rotational dynamics.

CHAPTER 23. SPIN AND ROTATION OPERATORS, STATES, AND DYNAMICS 1

Chapter 23. Spin and Rotation Operators, States, and Dynamics

23.1 2D Oscillation and 3D Rotation and Rotational Momentum

The relationship between the complex *U(2)* spinor-oscillator $\{x_1+ip_1, x_2+ip_2\}$ space and a three-dimensional *R(3)* spin-vector $\{ S_X, S_Y, S_Z \}$ or $\{ S_B, S_C, S_A \}$ space was first introduced by the Chapter 10 equation (10.5.1b). The preceding Sections 21.1. and 21.2 have described the *U(2)* operators and quantum 2-D oscillator eigensolutions generated by *U(2)* operators. Here we show the *R(3)* side of the story that deals with rotations in three-dimensions and the beginning of the quantum theory of angular momentum. It also completes the role of *U(2)* in quantum theory. This approach to angular momentum theory has parts that are generally credited to Jordan, Casimir, and Schwinger.

(a) Angular momentum generators by U(2) analysis

Each of the block matrices in (21.1.15c) can be written as linear combinations of representations of quantum angular momentum operators $\{ \mathbf{S}_X, \mathbf{S}_Y, \mathbf{S}_Z \}$ and the unit operator $\mathbf{S}_0 = \mathbf{1}$. The first one has been used many times and most recently in Sec. 21.1 in (21.1.19) to solve ($\upsilon=1$) or ($j=1/2$) oscillator.

$$\begin{pmatrix} A & B-iC \\ B+iC & D \end{pmatrix} = \frac{A+D}{2}\begin{pmatrix} 1 & 0 \\ 0 & 1 \end{pmatrix} + 2B\begin{pmatrix} 0 & \frac{1}{2} \\ \frac{1}{2} & 0 \end{pmatrix} + 2C\begin{pmatrix} 0 & -\frac{i}{2} \\ \frac{i}{2} & 0 \end{pmatrix} + (A-D)\begin{pmatrix} \frac{1}{2} & 0 \\ 0 & -\frac{1}{2} \end{pmatrix} \quad (23.1.1a)$$

The next block of (21.1.15c) is a 3-by-3 block used to solve ($\upsilon=2$) or ($j=1$) oscillation.

$$\begin{pmatrix} 2A & \sqrt{2}(B-iC) & \cdot \\ \sqrt{2}(B+iC) & A+D & \sqrt{2}(B-iC) \\ \cdot & \sqrt{2}(B+iC) & 2D \end{pmatrix} = (A+D)\begin{pmatrix} 1 & \cdot & \cdot \\ \cdot & 1 & \cdot \\ \cdot & \cdot & 1 \end{pmatrix} + 2B\begin{pmatrix} \cdot & \frac{\sqrt{2}}{2} & \cdot \\ \frac{\sqrt{2}}{2} & \cdot & \frac{\sqrt{2}}{2} \\ \cdot & \frac{\sqrt{2}}{2} & \cdot \end{pmatrix} + 2C\begin{pmatrix} \cdot & -i\frac{\sqrt{2}}{2} & \cdot \\ i\frac{\sqrt{2}}{2} & \cdot & -i\frac{\sqrt{2}}{2} \\ \cdot & i\frac{\sqrt{2}}{2} & \cdot \end{pmatrix} + (A-D)\begin{pmatrix} 1 & \cdot & \cdot \\ \cdot & 0 & \cdot \\ \cdot & \cdot & -1 \end{pmatrix}$$

The third block of (21.1.15c) is a 4-by-4 block is the ($\upsilon=3$) or ($j=3/2$) submatrix. (23.1.1b)

$$\begin{pmatrix} 3A & \sqrt{3}(B-iC) & & \\ \sqrt{3}(B+iC) & 2A+D & \sqrt{4}(B-iC) & \\ & \sqrt{4}(B+iC) & A+2D & \sqrt{3}(B-iC) \\ & & \sqrt{3}(B+iC) & 3D \end{pmatrix} =$$

$$= \frac{3(A+D)}{2}\begin{pmatrix} 1 & \cdot & \cdot & \cdot \\ \cdot & 1 & \cdot & \cdot \\ \cdot & \cdot & 1 & \cdot \\ \cdot & \cdot & \cdot & 1 \end{pmatrix} + 2B\begin{pmatrix} \cdot & \frac{\sqrt{3}}{2} & \cdot & \cdot \\ \frac{\sqrt{3}}{2} & \cdot & \frac{\sqrt{4}}{2} & \cdot \\ \cdot & \frac{\sqrt{4}}{2} & \cdot & \frac{\sqrt{3}}{2} \\ \cdot & \cdot & \frac{\sqrt{3}}{2} & \cdot \end{pmatrix} + 2C\begin{pmatrix} \cdot & -i\frac{\sqrt{3}}{2} & \cdot & \cdot \\ i\frac{\sqrt{3}}{2} & \cdot & -i\frac{\sqrt{4}}{2} & \cdot \\ \cdot & i\frac{\sqrt{4}}{2} & \cdot & -i\frac{\sqrt{3}}{2} \\ \cdot & \cdot & i\frac{\sqrt{3}}{2} & \cdot \end{pmatrix} + (A-D)\begin{pmatrix} \frac{3}{2} & \cdot & \cdot & \cdot \\ \cdot & \frac{1}{2} & \cdot & \cdot \\ \cdot & \cdot & -\frac{1}{2} & \cdot \\ \cdot & \cdot & \cdot & -\frac{3}{2} \end{pmatrix} \quad (23.1.1c)$$

All the block matrices have the form first introduced in (10.5.10). Here, we factor the *j-th* block.

$$\langle \mathbf{H} \rangle^{j-block} = 2j\Omega_0\langle \mathbf{1} \rangle^j + \Omega_X\langle \mathbf{s}_X \rangle^j + \Omega_Y\langle \mathbf{s}_Y \rangle^j + \Omega_Z\langle \mathbf{s}_Z \rangle^j$$

$$= 2j\Omega_0\langle \mathbf{1} \rangle^j + \left[(\Omega_X - i\Omega_Y)\langle \mathbf{s}_X + i\mathbf{s}_Y \rangle^j + (\Omega_X + i\Omega_Y)\langle \mathbf{s}_X - i\mathbf{s}_Y \rangle^j \right]/2 + \Omega_Z\langle \mathbf{s}_Z \rangle^j$$

where $\mathbf{S}_+ = \mathbf{S}_X + \mathrm{i}\,\mathbf{S}_Y$, and $\mathbf{S}_- = \mathbf{S}_X - \mathrm{i}\,\mathbf{S}_Y = \mathbf{S}_+^\dagger$ (23.1.2)

are called the *angular momentum raising operator* $\mathbf{S}_+$ and *lowering operator* $\mathbf{S}_-$.

Here the fundamental base state labeling will be electron spin-up and spin-dn, exclusively.

$$|1\rangle = \left|\uparrow\right\rangle = \left| \begin{array}{c} 1/2 \\ +1/2 \end{array} \right\rangle = \mathbf{a}_1^\dagger|0\rangle = \mathbf{a}_\uparrow^\dagger|0\rangle, \qquad |2\rangle = \left|\downarrow\right\rangle = \left| \begin{array}{c} 1/2 \\ -1/2 \end{array} \right\rangle = \mathbf{a}_2^\dagger|0\rangle = \mathbf{a}_\downarrow^\dagger|0\rangle. \tag{23.1.3}$$

The optical analog will be temporarily put aside. However, the oscillator state definition (21.1.14) of υ-boson states will be used with the connection relations (21.2.5) between *(j,m)* quanta involving total momentum *j* and sub-quantum *m* and oscillator quanta $(n_1 = j+m,\ n_2 = j-m)$ as follows.

$$|n_1 n_2\rangle = \frac{\left(\mathbf{a}_1^\dagger\right)^{n_1}\left(\mathbf{a}_2^\dagger\right)^{n_2}}{\sqrt{n_1!\,n_2!}}|0\,0\rangle = \frac{\left(\mathbf{a}_1^\dagger\right)^{j+m}\left(\mathbf{a}_2^\dagger\right)^{j-m}}{\sqrt{(j+m)!(j-m)!}}|0\,0\rangle = \left|\begin{smallmatrix} j \\ m \end{smallmatrix}\right\rangle \tag{23.1.4}$$

The *j*-blocks later turn out to be irreducible representations of *U(2)* or *R(3)*. So we will use the *D*-notation introduced in Section 3.6 as well as Dirac bracket notation to designate them. Starting with *j=1/2*

$$\langle \mathbf{s}_+ \rangle^{\frac{1}{2}} = D^{\frac{1}{2}}(\mathbf{s}_+) = D^{\frac{1}{2}}(\mathbf{s}_X + i\mathbf{s}_Y) = \begin{pmatrix} 0 & \frac{1}{2} \\ \frac{1}{2} & 0 \end{pmatrix} + i\begin{pmatrix} 0 & -\frac{i}{2} \\ \frac{i}{2} & 0 \end{pmatrix} = \begin{pmatrix} 0 & 1 \\ 0 & 0 \end{pmatrix} \tag{23.1.5a}$$

we see that $\mathbf{S}_+$ is represented by an *elementary projection operator* $\mathbf{e}_{12} = |1\rangle\langle 2| = \mathbf{P}_{12}$ first introduced in (3.1.25) and featured in (15.1.19). In Chapter 21, such operators were upgraded to creation-destruction operator combinations in (21.1.7). The $\mathbf{S}_+$ operators can be so written.

$$\mathbf{S}_+ = \mathbf{a}_1^\dagger\mathbf{a}_2 = \mathbf{a}_\uparrow^\dagger\mathbf{a}_\downarrow \ , \qquad \mathbf{S}_- = \left(\mathbf{a}_1^\dagger\mathbf{a}_2\right)^\dagger = \mathbf{a}_2^\dagger\mathbf{a}_1 = \mathbf{a}_\downarrow^\dagger\mathbf{a}_\uparrow \tag{23.1.5b}$$

They do their raising and lowering one-half quantum at a time. $\mathbf{S}_+$ destroys a down-spin ↓ and creates an up-spin ↑ in order to raise by one $\hbar$ unit of angular momentum. $\mathbf{S}_-$ does *vice-versa* to lower by one $\hbar$.

So also, the fundamental Hamilton-Pauli-Jordan representation of $\mathbf{S}_Z$ is

$$\langle \mathbf{S}_Z \rangle^{\frac{1}{2}} = D^{\frac{1}{2}}(\mathbf{S}_Z) = \begin{pmatrix} \frac{1}{2} & 0 \\ 0 & -\frac{1}{2} \end{pmatrix} \tag{23.1.5c}$$

and this leads to an $\mathbf{a}^\dagger\mathbf{a}$ form for it.

$$\mathbf{S}_Z = \frac{1}{2}\left(\mathbf{a}_1^\dagger\mathbf{a}_1 - \mathbf{a}_2^\dagger\mathbf{a}_2\right) = \frac{1}{2}\left(\mathbf{a}_\uparrow^\dagger\mathbf{a}_\uparrow - \mathbf{a}_\downarrow^\dagger\mathbf{a}_\downarrow\right) \tag{23.1.5d}$$

Oscillator matrix formulas (21.1.15a) give the following matrix elements of $\mathbf{S}_+$ and $\mathbf{S}_-$.

$$\begin{aligned} \mathbf{a}_1^\dagger\mathbf{a}_2|n_1 n_2\rangle = \sqrt{n_1+1}\sqrt{n_2}\,|n_1+1\ n_2-1\rangle \quad &\Rightarrow \quad \mathbf{S}_+\left|\begin{smallmatrix} j \\ m \end{smallmatrix}\right\rangle = \sqrt{j+m+1}\sqrt{j-m}\left|\begin{smallmatrix} j \\ m+1 \end{smallmatrix}\right\rangle \\ \mathbf{a}_2^\dagger\mathbf{a}_1|n_1 n_2\rangle = \sqrt{n_1}\sqrt{n_2+1}\,|n_1-1\ n_2+1\rangle \quad &\Rightarrow \quad \mathbf{S}_-\left|\begin{smallmatrix} j \\ m \end{smallmatrix}\right\rangle = \sqrt{j+m}\sqrt{j-m+1}\left|\begin{smallmatrix} j \\ m-1 \end{smallmatrix}\right\rangle \end{aligned} \tag{23.1.5e}$$

The diagonal $\mathbf{S}_Z$ operator is similarly given by a difference between number operators.

$$\left.\begin{aligned} \mathbf{a}_1^\dagger\mathbf{a}_1|n_1 n_2\rangle = n_1|n_1\ n_2\rangle \\ \mathbf{a}_2^\dagger\mathbf{a}_2|n_1 n_2\rangle = n_2|n_1\ n_2\rangle \end{aligned}\right\} \ \Rightarrow \ \mathbf{S}_Z\left|\begin{smallmatrix} j \\ m \end{smallmatrix}\right\rangle = \frac{1}{2}\left(\mathbf{a}_1^\dagger\mathbf{a}_1 - \mathbf{a}_2^\dagger\mathbf{a}_2\right)\left|\begin{smallmatrix} j \\ m \end{smallmatrix}\right\rangle = \frac{n_1-n_2}{2}\left|\begin{smallmatrix} j \\ m \end{smallmatrix}\right\rangle = m\left|\begin{smallmatrix} j \\ m \end{smallmatrix}\right\rangle \tag{23.1.5f}$$

This is Schwinger's derivation of the angular momentum operator irreducible representations. It is hard to imagine a simpler procedure for getting such important and general rules.

So the **H**-matrix blocks are once again combinations of group generators, in this case, they are called angular momentum generators $\mathbf{S}_K$ ("Jenerators" if you prefer to label them with **J**) . We list two operator representations beyond *j=1/2*, the spin-1 generators and then the spin-*3/2* generators.

$$D^1(\mathbf{S}_+)=D^1(\mathbf{S}_X+i\mathbf{S}_Y)=\begin{pmatrix} \cdot & \frac{\sqrt{2}}{2} & \cdot \\ \frac{\sqrt{2}}{2} & \cdot & \frac{\sqrt{2}}{2} \\ \cdot & \frac{\sqrt{2}}{2} & \cdot \end{pmatrix}+i\begin{pmatrix} \cdot & -i\frac{\sqrt{2}}{2} & \cdot \\ i\frac{\sqrt{2}}{2} & \cdot & -i\frac{\sqrt{2}}{2} \\ \cdot & i\frac{\sqrt{2}}{2} & \cdot \end{pmatrix}=\begin{pmatrix} \cdot & \sqrt{2} & \cdot \\ 0 & \cdot & \sqrt{2} \\ \cdot & 0 & \cdot \end{pmatrix},\quad D^1(\mathbf{S}_Z)=\begin{pmatrix} 1 & \cdot & \cdot \\ \cdot & 0 & \cdot \\ \cdot & \cdot & -1 \end{pmatrix} \qquad (23.1.6a)$$

$$D^{\frac{3}{2}}(\mathbf{S}_+)=\begin{pmatrix} \cdot & \sqrt{3} & \cdot & \cdot \\ 0 & \cdot & \sqrt{4} & \cdot \\ \cdot & 0 & \cdot & \sqrt{3} \\ \cdot & \cdot & 0 & \cdot \end{pmatrix}=\left(D^{\frac{3}{2}}(\mathbf{S}_-)\right)^\dagger \qquad D^{\frac{3}{2}}(\mathbf{S}_Z)=\begin{pmatrix} \frac{3}{2} & \cdot & \cdot & \cdot \\ \cdot & \frac{1}{2} & \cdot & \cdot \\ \cdot & \cdot & -\frac{1}{2} & \cdot \\ \cdot & \cdot & \cdot & -\frac{3}{2} \end{pmatrix} \qquad (23.1.6b)$$

Fourth on the list are the important "tensor" or spin-*2* generators. The pattern is becoming clear.

$$D^2(\mathbf{S}_+)=\begin{pmatrix} \cdot & \sqrt{4} & \cdot & \cdot & \cdot \\ 0 & \cdot & \sqrt{3} & \cdot & \cdot \\ \cdot & 0 & \cdot & \sqrt{3} & \cdot \\ \cdot & \cdot & 0 & \cdot & \sqrt{4} \\ \cdot & \cdot & \cdot & 0 & \cdot \end{pmatrix}=\left(D^2(\mathbf{S}_-)\right)^\dagger \qquad D^2(\mathbf{S}_Z)=\begin{pmatrix} 2 & \cdot & \cdot & \cdot & \cdot \\ \cdot & 1 & \cdot & \cdot & \cdot \\ \cdot & \cdot & 0 & \cdot & \cdot \\ \cdot & \cdot & \cdot & -1 & \cdot \\ \cdot & \cdot & \cdot & \cdot & -2 \end{pmatrix} \qquad (23.1.6c)$$

(1) Angular momentum commutation relations

Historically, the quantum theory of angular momentum began with the Hamilton-Jordan product relations $\sigma_\alpha\sigma_\beta=\delta_{\alpha\beta}+i\varepsilon_{\alpha\beta\gamma}\sigma_\gamma$ introduced back in Ch. 10. Here is the *commutator* form for $\mathbf{S}_\alpha=\sigma_\alpha/2$.

$$\mathbf{S}_\alpha\mathbf{S}_\beta - \mathbf{S}_\beta\mathbf{S}_\alpha = [\mathbf{S}_\alpha, \mathbf{S}_\beta] = i\,\varepsilon_{\alpha\beta\gamma}\,\mathbf{S}_\gamma \qquad (23.1.7a)$$

Matrices (23.1.6) satisfy (23.1.7a). More to the point, they satisfy the *eigen-commutation relations*.

$$[\mathbf{S}_Z, \mathbf{S}_+] = (+1)\mathbf{S}_+ \qquad [\mathbf{S}_Z, \mathbf{S}_-] = (-1)\mathbf{S}_- \qquad (23.1.7b)$$

These can be verified quickly using basic $[\mathbf{a}_m, \mathbf{a}^\dagger_n] = \delta_{mn}\mathbf{1}$ relations from (21.1.5), or even more quickly by doing elementary matrix or operator multiplication $\mathbf{e}_{jk}\,\mathbf{e}_{mn} = \delta_{km}\,\mathbf{e}_{jn}$ as in (15.1.19) or (3.1.25b).

$$[(\mathbf{e}_{11} - \mathbf{e}_{22})/2\,,\,\mathbf{e}_{12}] = +\mathbf{e}_{12}\,,\quad [(\mathbf{e}_{11} - \mathbf{e}_{22})/2\,,\,\mathbf{e}_{21}] = -\mathbf{e}_{21} \qquad (23.1.7c)$$

The same applies to the up-down commutation relation.

$$[\mathbf{S}_+, \mathbf{S}_-] = [\mathbf{e}_{12}\,,\,\mathbf{e}_{21}] = \mathbf{e}_{11} - \mathbf{e}_{22} = 2\,\mathbf{S}_Z \qquad (23.1.7d)$$

Such elementary considerations mean the old commutators aren't needed to derive matrices. But, they do provide insight into the idea of using operators to manage a diagonalization problem.

The main idea here is that if you can find a set of operators $(\mathbf{a}_m, \mathbf{a}^\dagger_n)$ such that a Hamiltonian **H** or any other operator such as $\mathbf{S}_Z$ will eigen-commute with all $(\mathbf{a}_m, \mathbf{a}^\dagger_n)$ as follows

$$[\,\mathbf{H},\mathbf{a}^\dagger_n\,]=\omega_n\,\mathbf{a}^\dagger_n\ ,\qquad [\,\mathbf{H},\mathbf{a}_m\,]=\omega_m\,\mathbf{a}_m\ , \tag{23.1.8a}$$

then the Hamiltonian will be a diagonal combination of number operators.

$$\mathbf{H}=\sum_{n=1}^{2}\omega_n\mathbf{a}^\dagger_n\mathbf{a}_n=\omega_1\mathbf{a}^\dagger_1\mathbf{a}_1+\omega_2\mathbf{a}^\dagger_2\mathbf{a}_2\approx\begin{pmatrix}\omega_1&0\\0&\omega_2\end{pmatrix} \tag{23.1.8b}$$

This is exactly what we achieve by diagonalizing the fundamental representation as in (21.1.20d). A fundamental eigenstate guarantees that all higher quantum matrices will be diagonal, too, and that the higher quantum states (23.1.4) have to be **H**-eigenvectors with the following eigenvalues.

$$\mathbf{H}\big|n_1n_2\big\rangle=\sum_{n=1}^{2}\omega_n\mathbf{a}^\dagger_n\mathbf{a}_n\big|n_1n_2\big\rangle=\big(\omega_1n_1+\omega_2n_2\big)\big|n_1n_2\big\rangle=\big(\omega_1(j+m)+\omega_2(j-m)\big)\Big|{}^{j}_{m}\Big\rangle \tag{23.1.8c}$$

(2) Angular momentum magnitude and uncertainty

There is one key angular momentum quantity besides $\mathbf{S}_Z$ that we generally find to be diagonal. This is the *angular momentum squared* $\mathbf{S}\circ\mathbf{S}$.

$$\mathbf{S}\circ\mathbf{S}=\mathbf{S}_X{}^2+\mathbf{S}_Y{}^2+\mathbf{S}_Z{}^2=(\mathbf{S}_+\mathbf{S}_-+\mathbf{S}_-\mathbf{S}_+)/2+\mathbf{S}_Z{}^2 \tag{23.1.9a}$$

You might think that its eigenvalue would just be the square j^2 of the angular quantum number j, but this is not so. For example, the $j=1/2$ fundamental matrices square up not to $(1/2)^2=1/4$ but to $3/4$.

$$D^{\frac12}\big(\mathsf{S}_X^2+\mathsf{S}_Y^2+\mathsf{S}_Z^2\big)=\frac14\begin{pmatrix}0&1\\1&0\end{pmatrix}\cdot\begin{pmatrix}0&1\\1&0\end{pmatrix}+\frac14\begin{pmatrix}0&-i\\i&0\end{pmatrix}\cdot\begin{pmatrix}0&-i\\i&0\end{pmatrix}+\frac14\begin{pmatrix}1&0\\0&-1\end{pmatrix}\cdot\begin{pmatrix}1&0\\0&-1\end{pmatrix}=\frac34\begin{pmatrix}1&0\\0&1\end{pmatrix}$$

(Remember that Pauli σ-matrices square to **1**.) In terms of **a**-operators the squared momentum operator is

$$\mathbf{S}\bullet\mathbf{S}=\frac14\Big[2\mathbf{a}^\dagger_1\mathbf{a}_2\mathbf{a}^\dagger_2\mathbf{a}_1+2\mathbf{a}^\dagger_2\mathbf{a}_1\mathbf{a}^\dagger_1\mathbf{a}_2+\big(\mathbf{a}^\dagger_1\mathbf{a}_1-\mathbf{a}^\dagger_2\mathbf{a}_2\big)\big(\mathbf{a}^\dagger_1\mathbf{a}_1-\mathbf{a}^\dagger_2\mathbf{a}_2\big)\Big]. \tag{23.1.9b}$$

Using $\mathbf{a}_m\mathbf{a}^\dagger_n=\mathbf{a}^\dagger_n\mathbf{a}_m+\delta_{mn}\mathbf{1}$ gives $\mathbf{S}\circ\mathbf{S}$ as number operators. (Normal order: *left←creation, destruct→right*.)

$$\mathbf{S}\bullet\mathbf{S}=\frac14\Big[2\big(\mathbf{a}^\dagger_2\mathbf{a}_2+\mathbf{1}\big)\mathbf{a}^\dagger_1\mathbf{a}_1+2\big(\mathbf{a}^\dagger_1\mathbf{a}_1+\mathbf{1}\big)\mathbf{a}^\dagger_2\mathbf{a}_2+\big(\mathbf{a}^\dagger_1\mathbf{a}_1-\mathbf{a}^\dagger_2\mathbf{a}_2\big)\big(\mathbf{a}^\dagger_1\mathbf{a}_1-\mathbf{a}^\dagger_2\mathbf{a}_2\big)\Big] \tag{23.1.9c}$$

So it is an eigenvector for all oscillator states. The eigenvalue formula is then found.

$$\begin{aligned}\mathbf{S}\bullet\mathbf{S}\big|n_1n_2\big\rangle&=\frac14\Big[2\big(n_2+1\big)n_1+2\big(n_1+1\big)n_2+\big(n_1-n_2\big)\big(n_1-n_2\big)\Big]\big|n_1n_2\big\rangle\\&=\frac14\Big[2n_1+2n_2+4n_1n_2+\big(n_1-n_2\big)\big(n_1-n_2\big)\Big]\big|n_1n_2\big\rangle\end{aligned} \tag{23.1.10a}$$

Using angular quanta in (23.1.4) where $n_1=j+m$ and $n_2=j-m$, an important general result follows.

$$\mathbf{S}\bullet\mathbf{S}\Big|{}^{j}_{m}\Big\rangle=\frac14\Big[2(j+m+1)(j-m)+2(j-m+1)(j+m)+4m^2\Big]\Big|{}^{j}_{m}\Big\rangle=j(j+1)\Big|{}^{j}_{m}\Big\rangle \tag{23.1.10b}$$

For large angular quanta the $\mathbf{S}\circ\mathbf{S}$ eigenvalue approaches j^2 , as you might guess, but the *magnitude of angular momentum* $|\mathbf{S}|$ approaches $j+1/2$. That little $1/2$ makes a lot of difference in the quantum world.

$$|\mathbf{S}|\Big|{}^{j}_{m}\Big\rangle=\sqrt{\mathbf{S}\bullet\mathbf{S}}\Big|{}^{j}_{m}\Big\rangle=\sqrt{j(j+1)}\Big|{}^{j}_{m}\Big\rangle\cong\Big(j+\frac12\Big)\Big|{}^{j}_{m}\Big\rangle \tag{23.1.10c}$$

This extra length of **S** is like a zero-point vibration in oscillators. Oscillator zero-point motion may be blamed on non-commuting operators **x** and **p** not being simultaneously diagonal eigenoperators. This prevents them from

both having zero values as discussed in Section 20.2(b4). So it is with angular momentum since non-commuting operators $\mathbf{S}_X$ and $\mathbf{S}_Y$ cannot either be diagonal eigenoperators if $\mathbf{S}_Z$ is diagonal as assumed. This prevents them from both having zero values and putting **S** right on the Z-axis.

Instead **S** has to "fuzz-out" in the $\mathbf{S}_X$ and $\mathbf{S}_Y$ plane defined by the $\mathbf{S}_Z$ eigenvalue of the magnetic quantum number *m*. As shown in Fig. 23.1.1 there is an angular "uncertainty cone" for each *j* and *m* value. The *angular momentum uncertainty angle* Θ^j_m is given by

$$\Theta^j_m = \arccos\left(\frac{m}{\sqrt{j(j+1)}}\right) \tag{23.1.11}$$

The resulting angles such as the ones shown in Fig. 23.1.2 for *j=30* are useful for estimating eigenvalues of angular momentum Hamiltonians just as the linear $\Delta x \Delta p$ uncertainty relation estimates power-law potential energies in (20.2.22). This "literal" interpretation of QTAM is often called *Dirac's vector model*.

(b) Generating rotations and rotational wavefunctions

A fundamental Euler transformation (10.A.1) is here written in three notations.

$$\begin{pmatrix} \langle 1|1'\rangle & \langle 1|2'\rangle \\ \langle 2|1'\rangle & \langle 2|2'\rangle \end{pmatrix} = \begin{pmatrix} \langle 1|\mathbf{R}(\alpha\beta\gamma)|1\rangle & \langle 1|\mathbf{R}(\alpha\beta\gamma)|2\rangle \\ \langle 2|\mathbf{R}(\alpha\beta\gamma)|1\rangle & \langle 2|\mathbf{R}(\alpha\beta\gamma)|2\rangle \end{pmatrix} = \begin{pmatrix} D^{1/2}_{11}(\alpha\beta\gamma) & D^{1/2}_{12}(\alpha\beta\gamma) \\ D^{1/2}_{21}(\alpha\beta\gamma) & D^{1/2}_{22}(\alpha\beta\gamma) \end{pmatrix}$$

$$= \begin{pmatrix} e^{-i\frac{\alpha+\gamma}{2}}\cos\frac{\beta}{2} & -e^{-i\frac{\alpha-\gamma}{2}}\sin\frac{\beta}{2} \\ e^{i\frac{\alpha-\gamma}{2}}\sin\frac{\beta}{2} & e^{i\frac{\alpha+\gamma}{2}}\cos\frac{\beta}{2} \end{pmatrix} \tag{23.1.12a}$$

This generates a transformation of the fundamental creation operators similar to (21.1.20d).

$$\begin{aligned} \mathbf{a}^\dagger_{1'} &= D^{1/2}_{11}(\alpha\beta\gamma)\mathbf{a}^\dagger_1 + D^{1/2}_{21}(\alpha\beta\gamma)\mathbf{a}^\dagger_2 = e^{-i\frac{\alpha+\gamma}{2}}\cos\frac{\beta}{2}\mathbf{a}^\dagger_1 + e^{i\frac{\alpha-\gamma}{2}}\sin\frac{\beta}{2}\mathbf{a}^\dagger_2, \\ \mathbf{a}^\dagger_{2'} &= D^{1/2}_{12}(\alpha\beta\gamma)\mathbf{a}^\dagger_1 + D^{1/2}_{22}(\alpha\beta\gamma)\mathbf{a}^\dagger_2 = -e^{-i\frac{\alpha-\gamma}{2}}\sin\frac{\beta}{2}\mathbf{a}^\dagger_1 + e^{i\frac{\alpha+\gamma}{2}}\cos\frac{\beta}{2}\mathbf{a}^\dagger_2, \end{aligned} \tag{23.1.12b}$$

The goal here is to find the corresponding transformation $D^j(\alpha\beta\gamma)$ matrix for a *2j*-quantum state (23.1.4). This will be the derivation of a very important result, the general formula for all irreducible representations (ireps) of *R(3)* and *U(2)*. A lot of theory (and labor-saving devices) depends on the next few steps

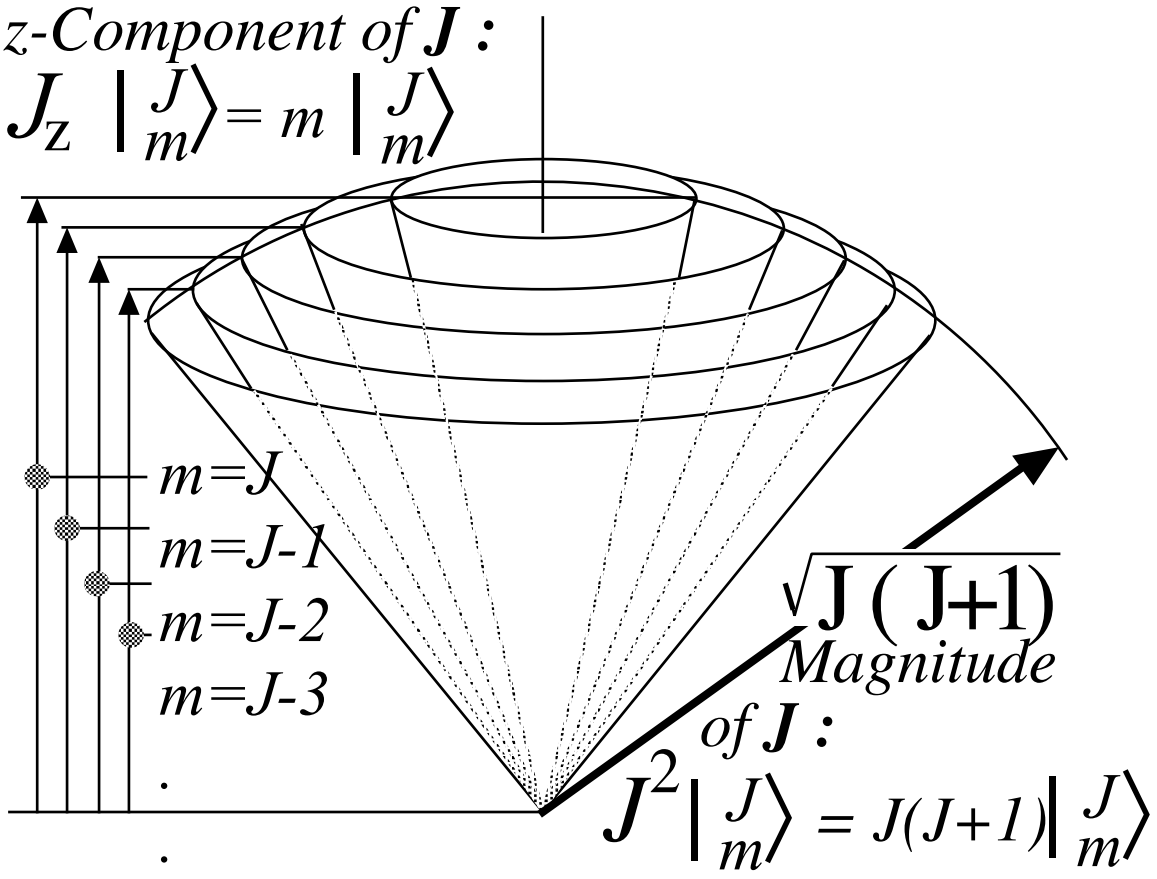

Fig. 23.1.1 Angular momentum uncertainty cones and geometry.

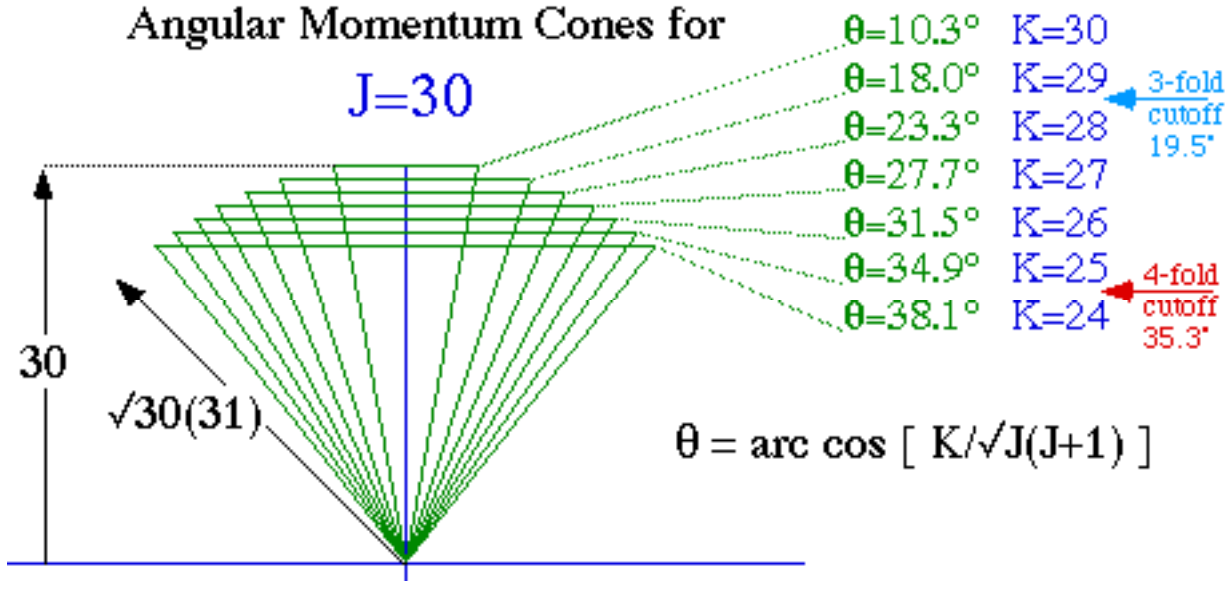

Fig. 23.1.2 Angular momentum uncertainty cones for j=30.

For a *2j*-quantum state (23.1.4) a rotation needs to be performed to the new "prime" basis.

$$\begin{aligned}\mathbf{R}(\alpha\beta\gamma)\left|\begin{smallmatrix} j \\ n \end{smallmatrix}\right\rangle &= \frac{\left(\mathbf{a}_{1'}^{\dagger}\right)^{j+n}\left(\mathbf{a}_{2'}^{\dagger}\right)^{j-n}}{\sqrt{(j+n)!(j-n)!}}|0\,0\rangle \\ &= \frac{\left(D_{11}\mathbf{a}_1^{\dagger}+D_{21}\mathbf{a}_2^{\dagger}\right)^{j+n}\left(D_{21}\mathbf{a}_1^{\dagger}+D_{22}\mathbf{a}_2^{\dagger}\right)^{j-n}}{\sqrt{(j+n)!(j-n)!}}|0\,0\rangle\end{aligned} \qquad (23.1.13)$$

Expanding the binomials yields a double sum over binomial coefficients $\binom{n}{k} = n!/\,k!(n-k)!$.

$$\mathbf{R}(\alpha\beta\gamma)\left|\begin{smallmatrix} j \\ n \end{smallmatrix}\right\rangle = \frac{\sum_{\ell}\sum_{k}\binom{j+n}{\ell}\left(D_{11}\mathbf{a}_1^{\dagger}\right)^{\ell}\left(D_{21}\mathbf{a}_2^{\dagger}\right)^{j+n-\ell}\binom{j-n}{k}\left(D_{12}\mathbf{a}_1^{\dagger}\right)^{k}\left(D_{22}\mathbf{a}_2^{\dagger}\right)^{j-n-k}}{\sqrt{(j+n)!(j-n)!}}|0\,0\rangle$$

$$= \sqrt{(j+n)!(j-n)!}\sum_{\ell}\sum_{k}\frac{\left(D_{11}\mathbf{a}_1^{\dagger}\right)^{\ell}\left(D_{21}\mathbf{a}_2^{\dagger}\right)^{j+n-\ell}\left(D_{12}\mathbf{a}_1^{\dagger}\right)^{k}\left(D_{22}\mathbf{a}_2^{\dagger}\right)^{j-n-k}}{\ell!(j+n-\ell)!k!(j-n-k)!}|0\,0\rangle$$

$$= \sqrt{(j+n)!(j-n)!}\sum_{\ell}\sum_{k}\frac{\left(D_{11}\right)^{\ell}\left(D_{21}\right)^{j+n-\ell}\left(D_{12}\right)^{k}\left(D_{22}\right)^{j-n-k}}{\ell!(j+n-\ell)!k!(j-n-k)!}\left(\mathbf{a}_1^{\dagger}\right)^{\ell+k}\left(\mathbf{a}_2^{\dagger}\right)^{2j-\ell-k}|0\,0\rangle$$

We replace the $\mathbf{a}^{\dagger}$-operator powers with the *j-m* and *j+m* forms they had in the beginning.

$$j+m = \ell + k \;,\; j - m = 2j - \ell - k \quad \text{or,} \quad \ell = j + m - k$$

The sum over ℓ becomes a sum over *m*.

$$\mathbf{R}(\alpha\beta\gamma)\left|\begin{smallmatrix} j \\ n \end{smallmatrix}\right\rangle = \sqrt{(j+n)!(j-n)!}\sum_{m}\sum_{k}\frac{\left(D_{11}\right)^{j+m-k}\left(D_{21}\right)^{n-m+k}\left(D_{12}\right)^{k}\left(D_{22}\right)^{j-n-k}}{(j+m-k)!(n-m+k)!k!(j-n-k)!}\left(\mathbf{a}_1^{\dagger}\right)^{j+m}\left(\mathbf{a}_2^{\dagger}\right)^{j-m}|0\,0\rangle$$

$$= \sqrt{(j+n)!(j-n)!}\sum_{m}\sum_{k}\frac{\sqrt{(j+m)!(j-m)!}\left(D_{11}\right)^{j+m-k}\left(D_{21}\right)^{n-m+k}\left(D_{12}\right)^{k}\left(D_{22}\right)^{j-n-k}}{(j+m-k)!(n-m+k)!k!(j-n-k)!}\left|\begin{smallmatrix} j \\ m \end{smallmatrix}\right\rangle$$

(23.1.14)

The resulting general *irreducible representation of U(2)* is the following.

$$\left\langle\begin{smallmatrix} j \\ m \end{smallmatrix}\right|\mathrm{R}(\alpha\beta\gamma)\left|\begin{smallmatrix} j \\ n \end{smallmatrix}\right\rangle = D^{j}_{m,n}(\alpha\beta\gamma) =$$

$$\sqrt{(j+n)!(j-n)!}\sqrt{(j+m)!(j-m)!}\sum_{k}\frac{\left(D_{11}\right)^{j+m-k}\left(D_{21}\right)^{n-m+k}\left(D_{12}\right)^{k}\left(D_{22}\right)^{j-n-k}}{(j+m-k)!(n-m+k)!k!(j-n-k)!}$$

(23.1.15a)

Inserting fundamental *D*-values from Euler rotation (23.1.12), simplifies the irep a little.

The result is a general *SU(2) irreducible representation for Euler angles (αβγ)*. It's a powerful result!

$$\left\langle {}^{j}_{m}\left|\mathbf{R}(\alpha\beta\gamma)\right|{}^{j}_{n}\right\rangle = D^{j}_{m,n}(\alpha\beta\gamma) =$$

$$\sqrt{(j+n)!(j-n)!}\sqrt{(j+m)!(j-m)!}\frac{\sum_k (-1)^k \left(\cos\frac{\beta}{2}\right)^{2j+m-n-2k}\left(\sin\frac{\beta}{2}\right)^{n-m+2k} e^{-i(m\alpha+n\gamma)}}{(j+m-k)!(n-m+k)!k!(j-n-k)!} \quad (23.1.15b)$$

(The Darboux angle representation is left as an exercise.) The *k*-sum is done over all positive integral values of *k* such that none of the denominator factors contain a negative integer. So *k* ranges between zero or *m-n* (whichever is *largest*) up to *j-m* or *j-n* (whichever is *least*). The phase factor involving α and γ angles is best left to be inserted later as shown in the *j = 1* example below.

$$D^1(\alpha\beta\gamma) = \begin{pmatrix} e^{-i\alpha} & . & . \\ . & 1 & . \\ . & . & e^{i\alpha} \end{pmatrix} \begin{pmatrix} \frac{1+\cos\beta}{2} & \frac{-\sin\beta}{\sqrt{2}} & \frac{1-\cos\beta}{2} \\ \frac{\sin\beta}{\sqrt{2}} & \cos\beta & \frac{-\sin\beta}{\sqrt{2}} \\ \frac{1-\cos\beta}{2} & \frac{\sin\beta}{\sqrt{2}} & \frac{1+\cos\beta}{2} \end{pmatrix} \begin{pmatrix} e^{-i\gamma} & . & . \\ . & 1 & . \\ . & . & e^{i\gamma} \end{pmatrix}$$

$$= \begin{pmatrix} e^{-i\alpha}\frac{1+\cos\beta}{2}e^{-i\gamma} & e^{-i\alpha}\frac{-\sin\beta}{\sqrt{2}} & e^{-i\alpha}\frac{1-\cos\beta}{2}e^{i\gamma} \\ \frac{\sin\beta}{\sqrt{2}}e^{-i\gamma} & \cos\beta & \frac{-\sin\beta}{\sqrt{2}}e^{i\gamma} \\ e^{i\alpha}\frac{1-\cos\beta}{2}e^{-i\gamma} & e^{i\alpha}\frac{\sin\beta}{\sqrt{2}} & e^{i\alpha}\frac{1+\cos\beta}{2}e^{i\gamma} \end{pmatrix} \quad (23.1.15c)$$

Here half-angle identities $\cos^2\frac{\beta}{2} = \frac{1+\cos\beta}{2}$, $\sin^2\frac{\beta}{2} = \frac{1-\cos\beta}{2}$, $\sin\frac{\beta}{2}\cos\frac{\beta}{2} = \frac{\sin\beta}{2}$, are used. The three Euler factors of the **R**(α)**R**(β)**R**(γ) form in (10.A.1) shown by Fig. 10.A.1. Below we list the tensor *(j=2)* irep.

$$D^2(\alpha\beta 0) = \left(\begin{array}{ccc|c|ccc} e^{-i2\alpha}\left(\frac{1+\cos\beta}{2}\right)^2 & e^{-i2\alpha}\left(\frac{1+\cos\beta}{2}\right)\sin\beta & \sqrt{\frac{3}{8}}e^{-i2\alpha}\sin^2\beta & e^{-i2\alpha}\left(\frac{1+\cos\beta}{2}\right)\sin\beta & e^{-i2\alpha}\left(\frac{1-\cos\beta}{2}\right)^2 \\ e^{-i\alpha}\left(\frac{1+\cos\beta}{2}\right)\sin\beta & e^{-i\alpha}\left(\frac{1+\cos\beta}{2}\right)(2\cos\beta-1) & -\sqrt{\frac{3}{2}}e^{-i\alpha}\sin\beta\cos\beta & e^{-i\alpha}\left(\frac{1-\cos\beta}{2}\right)(2\cos\beta+1) & -e^{-i\alpha}\left(\frac{1-\cos\beta}{2}\right)\sin\beta \\ \sqrt{\frac{3}{8}}\sin^2\beta & \sqrt{\frac{3}{2}}\sin\beta\cos\beta & \frac{3\cos^2\beta-1}{2} & \sqrt{\frac{3}{2}}\sin\beta\cos\beta & \sqrt{\frac{3}{8}}\sin^2\beta \\ e^{i\alpha}\left(\frac{1+\cos\beta}{2}\right)\sin\beta & e^{i\alpha}\left(\frac{1-\cos\beta}{2}\right)(2\cos\beta+1) & \sqrt{\frac{3}{2}}e^{i\alpha}\sin\beta\cos\beta & e^{i\alpha}\left(\frac{1+\cos\beta}{2}\right)(2\cos\beta-1) & -e^{i\alpha}\left(\frac{1+\cos\beta}{2}\right)\sin\beta \\ e^{i2\alpha}\left(\frac{1-\cos\beta}{2}\right)^2 & e^{i2\alpha}\left(\frac{1-\cos\beta}{2}\right)\sin\beta & \sqrt{\frac{3}{8}}e^{i2\alpha}\sin^2\beta & e^{i2\alpha}\left(\frac{1+\cos\beta}{2}\right)\sin\beta & e^{i2\alpha}\left(\frac{1+\cos\beta}{2}\right)^2 \end{array}\right) \quad (23.1.15d)$$

Here the third Euler "twist" angle was set to zero, but it is easily reinserted column by column. That angle is not needed for atomic electronic wavefunctions since they are completely described by two polar angles of azimuth ϕ =α and the polar angle θ=β. For this case only the center (*n=0*) column is used, but its conjugate with factor $\sqrt{(2l+1/4\pi)}$ gives a normalized and properly phased set of *spherical harmonics* Y^{ℓ}_{m}.

$$D^{\ell}_{m,n=0}{}^{*}(\phi\theta 0)\sqrt{2\ell+1/4\pi} = Y^{\ell}_{m}(\phi\theta) \quad (23.1.16)$$

Such is the power of algebraic methods that solve countless differential equations all at once.

(c) Rotational R(3) and U(2) wavefunctions and projectors

One thing that uses the *SU(2)* ireps is the *Wigner-Weyl projector* $\mathbf{P}^{j}_{m,n}$. Such a projector was introduced in (15.1.20d) for the D_3 subgroup of *R(3)*. The following applies to all of *SU(2)* and *R(3)*.

$$\mathbf{P}^{j}_{m,n} = \frac{\ell^j}{N}\int d(\alpha\beta\gamma)\, D^{j*}_{m,n}(\alpha\beta\gamma)\mathbf{R}(\alpha\beta\gamma) \tag{23.1.17a}$$

Here: $\ell^{\,j} = 2j+1$ (23.1.17b)

is the irreducible representation dimension or *multiplet degeneracy* for *SU(2)* or *R(3)* symmetry

For *SU(2)* and *R(3)*, the sum over rotations is now an integral over the Euler angles *(*αβγ*)*. For integral-*j=0, 1, 2,..* the *R(3)* integral is used. Polar angle β only ranges from 0 to π.

$$for\ R(3): \frac{\ell^j}{N}\int d(\alpha\beta\gamma) = \frac{2j+1}{8\pi^2}\int_0^{2\pi} d\alpha \int_0^{\pi} d\beta \sin\beta \int_0^{2\pi} d\gamma \ = 2j+1 \tag{`(23.1.17c)}$$

For half-integral-*j=1/2, 3/2, 5/2,..* the *SU(2)* integral is used. β now ranges from -π to π.

$$for\ SU(2): \frac{\ell^j}{N}\int d(\alpha\beta\gamma) = \frac{2j+1}{16\pi^2}\int_0^{2\pi} d\alpha \int_{-\pi}^{\pi} d\beta \sin\beta \int_0^{2\pi} d\gamma \ = 2j+1 \tag{23.1.17d}$$

The latter is twice as big as the *R(3)* domain since the polar angle β has to cover its negative territory in the *SU(2)* world. This was shown when a full 4π *SU(2)* rotation was demonstrated in Fig.10.A.5.

As explained in the discussion of Fig. 10.A.4, *(*α, β*)* are azimuth α and polar β angles for the body frame zenith relative to the lab frame, while *(*–β, –γ*)* are polar angle –β and azimuth –γ for the lab zenith in the body frame. From the start we will treat both the internal or dual description and the external or laboratory reference frames on mostly equal footing. I say "mostly" because the body frame is not the one that is familiar to most students of atomic physics. Electrons are *quantum point* particles.

However, for molecular or nuclear theory the concept of a *quantum body* is very much a part of things, and it needs an "inside" azimuth –γ or "twist" angle to define its orientation. Atomic points, electrons and nuclei, are not allowed to "twist" so only one kind of azimuth α is needed.

Eigenstates of angular momentum are built from projected initial position states |000⟩.

$$\left|{}^{j}_{m,n}\right\rangle = \frac{\mathbf{P}^{j}_{m,n}|000\rangle}{\sqrt{\ell^j}} = \frac{1}{N}\int d(\alpha\beta\gamma)\, D^{j*}_{m,n}(\alpha\beta\gamma)\mathbf{R}(\alpha\beta\gamma)|000\rangle\sqrt{\ell^j}$$
$$= \frac{1}{N}\int d(\alpha\beta\gamma)\, D^{j*}_{m,n}(\alpha\beta\gamma)\sqrt{\ell^j}\,|\alpha\beta\gamma\rangle \tag{23.1.18}$$

The angular position states of a body are defined by a *rotational duality relativity relation* like (15.3.8)

$$\mathbf{R}(\alpha\beta\gamma)|000\rangle = |\alpha\beta\gamma\rangle = \bar{\mathbf{R}}^{\dagger}(\alpha\beta\gamma)|000\rangle \tag{23.1.19a}$$

This relates ordinary lab-based operators $\mathbf{R}(\alpha\beta\gamma)$ to body-based operators $\bar{\mathbf{R}}(\alpha\beta\gamma)$ that share exactly the same group properties but move the lab relative to their body frame instead of *vice-versa*. It is important to remember that these two sets are mutually exclusive (disjoint) and mutually commuting.

$$\mathbf{R}(\alpha\beta\gamma)\bar{\mathbf{R}}(\alpha'\beta'\gamma') = \bar{\mathbf{R}}(\alpha'\beta'\gamma')\mathbf{R}(\alpha\beta\gamma) \quad \text{for all } (\alpha\beta\gamma) \text{ and } (\alpha'\beta'\gamma') \tag{23.1.19b}$$

The two kinds of operators work different sides of the street. Analogous to (15.3.10) their effect is cleanly split between the left hand (lab-*m*) and right hand (body-*n*) quantum numbers.

$$\mathbf{R}(\alpha\beta\gamma)\left|{}^{j}_{m,n}\right\rangle=\sum_{m'=-j}^{j}D^{j}_{m',m}(\alpha\beta\gamma)\left|{}^{j}_{m',n}\right\rangle \qquad \bar{\mathbf{R}}(\alpha\beta\gamma)\left|{}^{j}_{m,n}\right\rangle=\sum_{n'=-j}^{j}D^{j*}_{n',n}(\alpha\beta\gamma)\left|{}^{j}_{m,n'}\right\rangle$$

(23.1.20a) (23.1.20b)

Note how body operators act in a reverse or conjugated sense. They view positive momentum as the lab spinning in a negative or clockwise sense. The same applies to the generators $\mathbf{J}_Z$ or $\mathbf{S}_Z$ of *SU(2)* or *R(3)*.

$$\mathbf{S}_Z\left|{}^{j}_{m,n}\right\rangle=m\left|{}^{j}_{m,n}\right\rangle \qquad \bar{\mathbf{S}}_Z\left|{}^{j}_{m,n}\right\rangle=-n\left|{}^{j}_{m,n}\right\rangle$$

(23.1.20c) (23.1.20d)

The reversed sign is regarded as a nuisance, so it is often customary to define *reversed momentum operators* that give a positive sign.

$$\mathbf{S}_{\bar{Z}}\left|{}^{j}_{m,n}\right\rangle=+n\left|{}^{j}_{m,n}\right\rangle \qquad \mathbf{S}_{\bar{Z}}=-\bar{\mathbf{S}}_Z \qquad (23.1.20b)$$

As an example of a rotor spectrum consider the Hamiltonian of a symmetric top molecule.

$$\mathbf{H}_{symmetric\ top}=B\mathbf{J}^2_{\bar{X}}+B\mathbf{J}^2_{\bar{Y}}+A\mathbf{J}^2_{\bar{Z}} \qquad (23.1.21a)$$

where the constants are inverse moments of inertia.

$$\frac{1}{2I_{\bar{X}}}=B=\frac{1}{2I_{\bar{Y}}}\ , \qquad A=\frac{1}{2I_{\bar{Z}}} \qquad (23.1.21b)$$

This Hamiltonian can be rewritten in terms of two commuting observables, the J_Z and J^2 operators.

$$\mathbf{H}_{symmetric\ top}=B\mathbf{J}^2_{\bar{X}}+B\mathbf{J}^2_{\bar{Y}}+B\mathbf{J}^2_{\bar{Z}}+(A-B)\mathbf{J}^2_{\bar{Z}}=B\mathbf{J}\bullet\mathbf{J}+(A-B)\mathbf{J}^2_{\bar{Z}} \qquad (23.1.21c)$$

The eigenvalue spectrum is given here and plotted in Fig. 23.1.3.

$$\begin{aligned}\mathbf{H}_{symmetric\ top}\left|{}^{j}_{m,n}\right\rangle&=B\mathbf{J}\bullet\mathbf{J}+(A-B)\mathbf{J}^2_{\bar{Z}}\left|{}^{j}_{m,n}\right\rangle\\&=\left[BJ(J+1)+(A-B)n^2\right]\left|{}^{j}_{m,n}\right\rangle\end{aligned} \qquad (23.1.21d)$$

The rotational j-levels are spaced quadratically like an elementary Bohr or Bloch problem with no potential, but the levels are split by the asymmetry of the rotor. If the rotor is a discus shape or *oblate top* its splittings are negative as in the left hand side of Fig. 23.1.3. If it is a sausage shape or *prolate top*, its splittings are positive as shown on the right hand side.

Each *n-stack* of the eigenvalue spectrum is quadratic like the elementary Bohr rotor. However, n stops at j and the degeneracy is more than 1 or 2 of the Bohr singlet or doublet levels. Even the $n=0$ levels are $2j+1$-fold degenerate and if n is non-zero the degeneracy is $4j+2$. The degeneracy for the case $(A=B)$ is a huge $(2j+1)^2 = 0, 9, 25, 49,...$ for $j= 0, 1, 2, 3, ...$ This case is known as a *spherical top* and has the super symmetry $R(3)*R(3)$ similar to D_3*D_3 introduced in Sec. 15.4.(2). Once again, this is a simple eigenvalue spectrum with a great variety of orthogonal wavefunctions hiding behind practically every level. It is necessary to understand the shape and symmetry, both global and local, of these waves in order to use them for understanding physics. Next we consider a few simple but important examples.

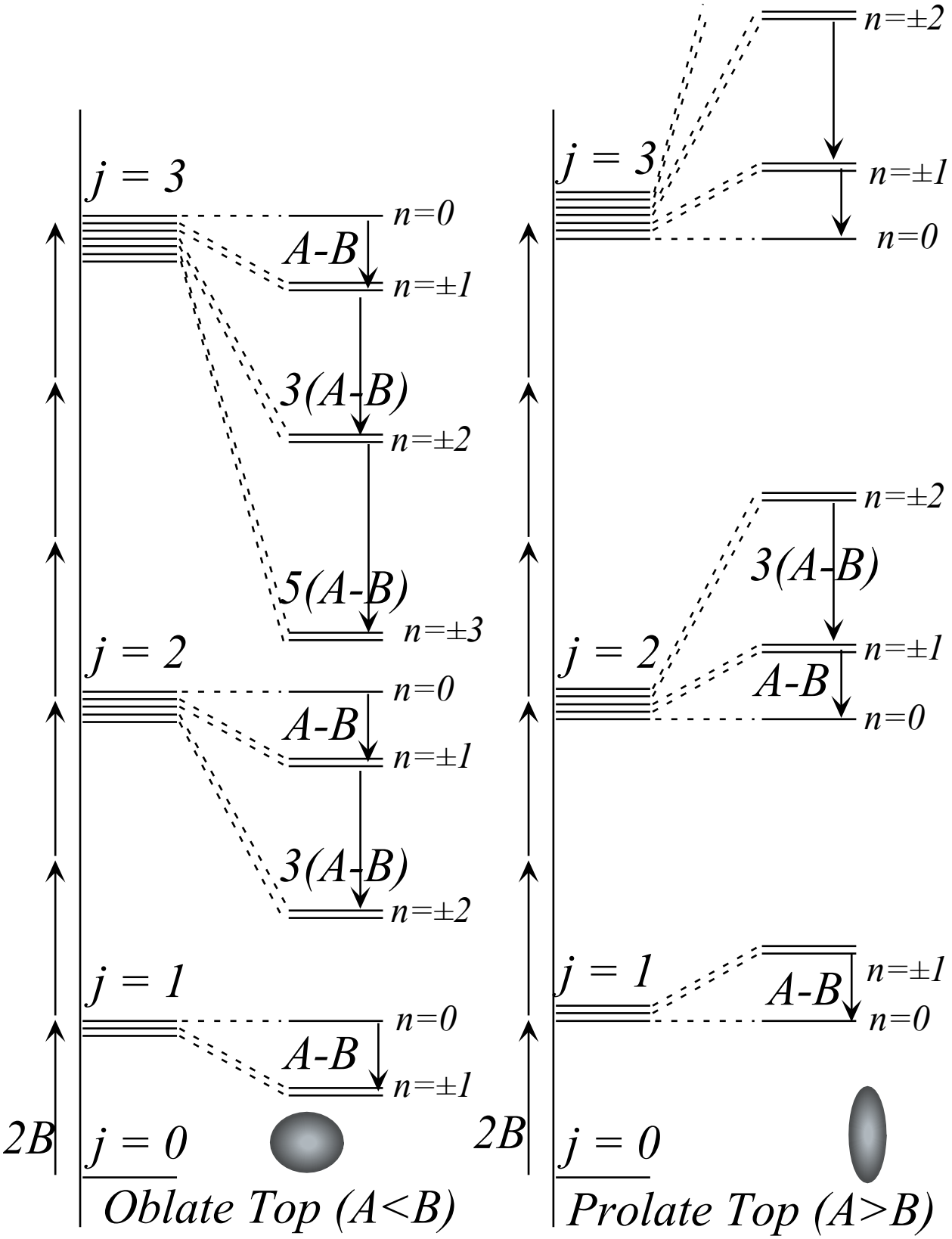

Fig. 23.1.3 Quantum rotor levels for j=0, 1, 2, 3,...

23.2 Structure and Applications of SU(2)–R(3) D-Functions

The D-matrix functions $D^j_{mn}(\alpha,\beta,\gamma)$ of Euler angles (α,β,γ) derived in 23.1.15 are extremely powerful stuff and serve many purposes. Their role as wavefunctions that go with the symmetric molecular rotor energy levels in Fig. 23.1.3 is just the first of many applications. Here we will discuss the molecular waves but also their most well known role as rotational transformation matrices for *spin-j polarization analysis*. Indeed, we have come full circle now from the discussion of spin-*1/2* and optical polarization matrices first introduced in Chapter 1. (23.1.15) is the generalization of the fundamental matrix

$$\mathrm{D}^{j=1/2}_{m,n}(0,\beta,0)=\begin{pmatrix}\langle\uparrow|\uparrow'\rangle & \langle\uparrow|\downarrow'\rangle\\ \langle\downarrow|\uparrow'\rangle & \langle\downarrow|\downarrow'\rangle\end{pmatrix}=\begin{pmatrix}\cos\beta/2 & -\sin\beta/2\\ \sin\beta/2 & \cos\beta/2\end{pmatrix}, \tag{23.2.1a}$$

introduced in (1.2.13) and related to the optical polarization (2-D oscillator) fundamental matrix

$$D^{j=1/2}_{m,n}(0,2\theta,0)=\begin{pmatrix}\langle x|x'\rangle & \langle x|y'\rangle\\ \langle y|x'\rangle & \langle y|y'\rangle\end{pmatrix}=\begin{pmatrix}\cos\theta & -\sin\theta\\ \sin\theta & \cos\theta\end{pmatrix}, \tag{23.2.1b}$$

first shown in (1.2.1). There as here we shall be first concerned with the behavior of the transformation *vis-à-vis* the middle or polar Euler angle β and leave for later discussion of the comparatively simpler functional behavior of lab azimuth α and body azimuth γ.

(a) Polarization analysis

Suppose a spin-j state $|^j_m\rangle$ with lab z-component-m is rotated by (23.1.20a) to give the following.

$$\mathbf{R}(\alpha\beta\gamma)\left|\begin{smallmatrix}j\\m\end{smallmatrix}\right\rangle=\sum_{j'=0}^{\infty}\sum_{m'=-j'}^{j'}\left|\begin{smallmatrix}j'\\m'\end{smallmatrix}\right\rangle\left\langle\begin{smallmatrix}j'\\m'\end{smallmatrix}\right|\mathbf{R}(\alpha\beta\gamma)\left|\begin{smallmatrix}j\\m\end{smallmatrix}\right\rangle \tag{23.2.2}$$

A rotation cannot change total spin-j so the completeness sum reduces to just $2j+1$ terms of D-matrices.

$$\mathbf{R}(\alpha\beta\gamma)\left|\begin{smallmatrix}j\\m\end{smallmatrix}\right\rangle=\sum_{m'=-j}^{j}\left|\begin{smallmatrix}j\\m'\end{smallmatrix}\right\rangle\left\langle\begin{smallmatrix}j\\m'\end{smallmatrix}\right|\mathbf{R}(\alpha\beta\gamma)\left|\begin{smallmatrix}j\\m\end{smallmatrix}\right\rangle=\sum_{m'=-j}^{j}\left|\begin{smallmatrix}j\\m'\end{smallmatrix}\right\rangle D^j_{m'm}(\alpha\beta\gamma) \tag{23.2.3a}$$

The overlap of this state with its unrotated brethren is exactly equal to the corresponding D-matrix element.

$$\left\langle\begin{smallmatrix}j'\\m'\end{smallmatrix}\right|\mathbf{R}(\alpha\beta\gamma)\left|\begin{smallmatrix}j\\m\end{smallmatrix}\right\rangle=\delta^{j'j}D^j_{m'm}(\alpha\beta\gamma)=\left\langle\begin{smallmatrix}j'\\m'\end{smallmatrix}\right|\left.\begin{smallmatrix}j\\m\end{smallmatrix}\right\rangle_R \tag{23.2.3b}$$

Here we ignore any hidden or internal quantum numbers such as the body-z-component n.

As in Chapter 1, let us imagine some sort of magnetic beam sorter that can sort a beam into separate beams of states $|^j_m\rangle$ as shown in Fig. 23.2.1. Each of $2j+1$ beams that come out contain particles that have "chosen" to change entirely from the initial state $\mathbf{R}(\alpha,\beta,\gamma)|^j_m\rangle$ entering on the right into a particular final $|^j_{m'}\rangle$ state emerging on the left.

In Fig. 23.2.1 the total spin is $(j=2)$, and so there are $2j+1=5$ possible input and output channels. In the figure all input channels except the $(m=1)$-channel have been filtered from the output of the first sorter. The first sorter, shown on the extreme upper right hand side, is rotated by an angle β so it produces states $\mathbf{R}(0,\beta,0)|^2_m\rangle$ of which only $\mathbf{R}(0,\beta,0)|^2_1\rangle$ is fed into the next analyzer. Each beam is indicated by angular-momentum cones from Fig. 23.1.1 belonging to $j=2$ states. Note that the $m'=-1$ plot peaks at β=π.

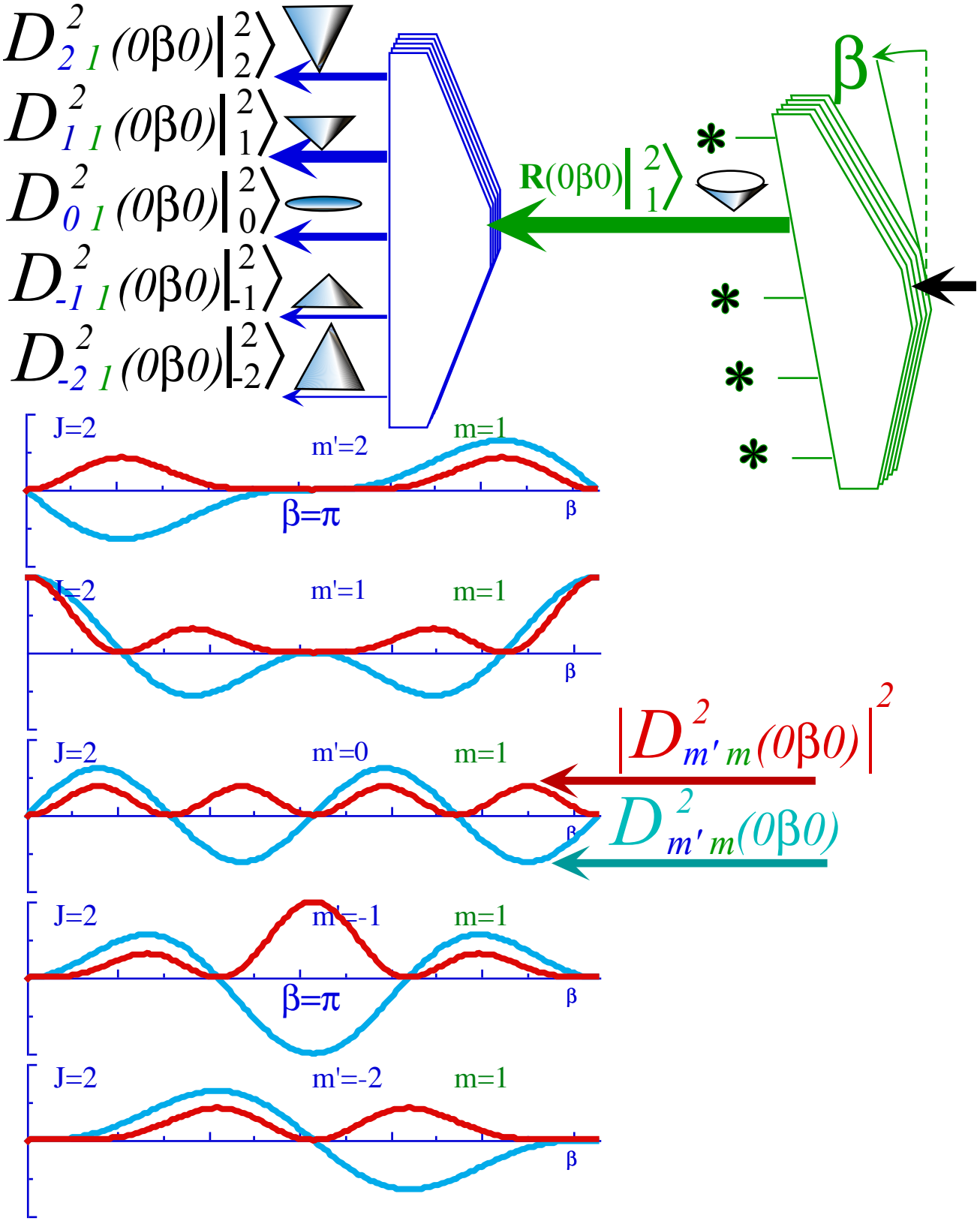

Fig. 23.2.1 (j=2)-Polarization analysis. Plots of D-amplitude and probability for each channel.

The fact that a $|^2_1\rangle$ cone tipped over by *180°* (β=π) is the same as a $|^2_{-1}\rangle$ cone is reassuring. Flipping the system should flip the momentum from *m=1* to *m'=-1*.

To gain a better picture of the *D*-amplitudes and the polarization process, Fig. 23.2.2 shows plots as the function of *m'* instead of β for a ten-times higher value *j=20* of spin magnitude. Note particularly how the lips of the β-tipped angular momentum cones project onto the z-axis a region of higher probability or wave amplitude. As β rotates, a "semi-classical region" follows underneath the cone base.

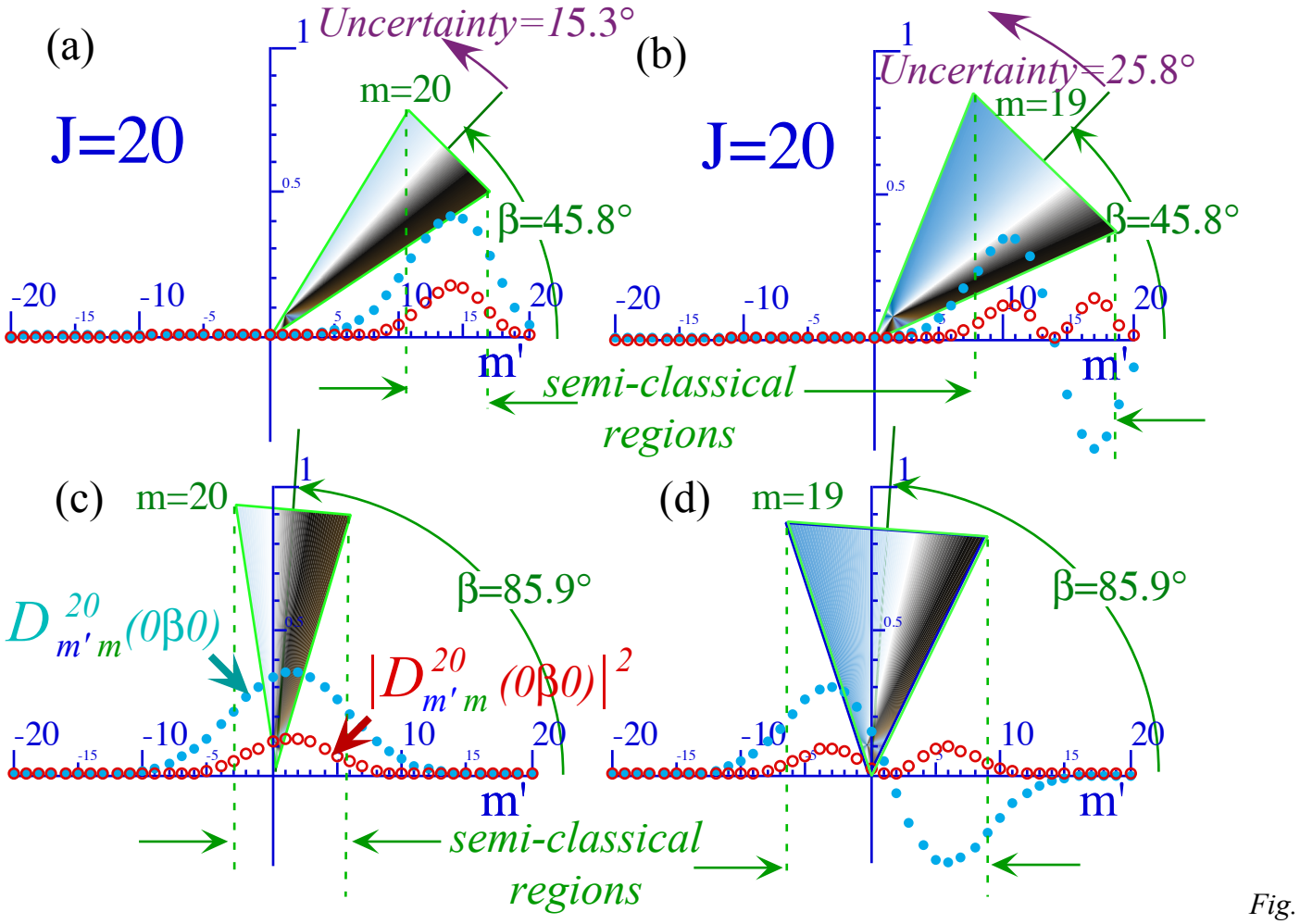

Fig. 23.2.2 (j=20)-Polarization analysis. m'-Plots of D-amplitude and probability for each channel.

Each dot in the wave or probability plot of Fig. 23.2.2(a) and 23.2.2(c) corresponds to a $D^{20}_{m'20}(0\beta 0)$ or $|D^{20}_{m'20}(0\beta 0)|^2$ value for a different *m'*-channel and represents an entirely different function of angle β=*45.8°* or β=*45.8°*, respectively. Yet, the dots form a curve that resembles a one-dimensional Gauss-like wavefunction! Fig. 23.2.2(b) and 23.2.2(d) plot a $D^{20}_{m'19}(0\beta 0)$ or $|D^{20}_{m'19}(0\beta 0)|^2$ in a similar fashion and form what looks like the wave of the first excited 1-D oscillator Gaussian! In each case the cone limbs or lips project what appear to be classical turning points of this 1-D discrete wave.

Polarization analysis for integral and half-integral spin uses the same *D*-function formula (23.1.15). However, there is one important difference as seen by comparing the matrix plots of *j=1/2*, and *j=1*, in Fig. 23.2.3(a-b) below. These are simply plots of (23.2.1a) and (23.1.15c). Both plots give similar periodic functions of period 2π for probability. But, the spin-*1/2* amplitudes change sign after a $\beta=2\pi$ rotation.

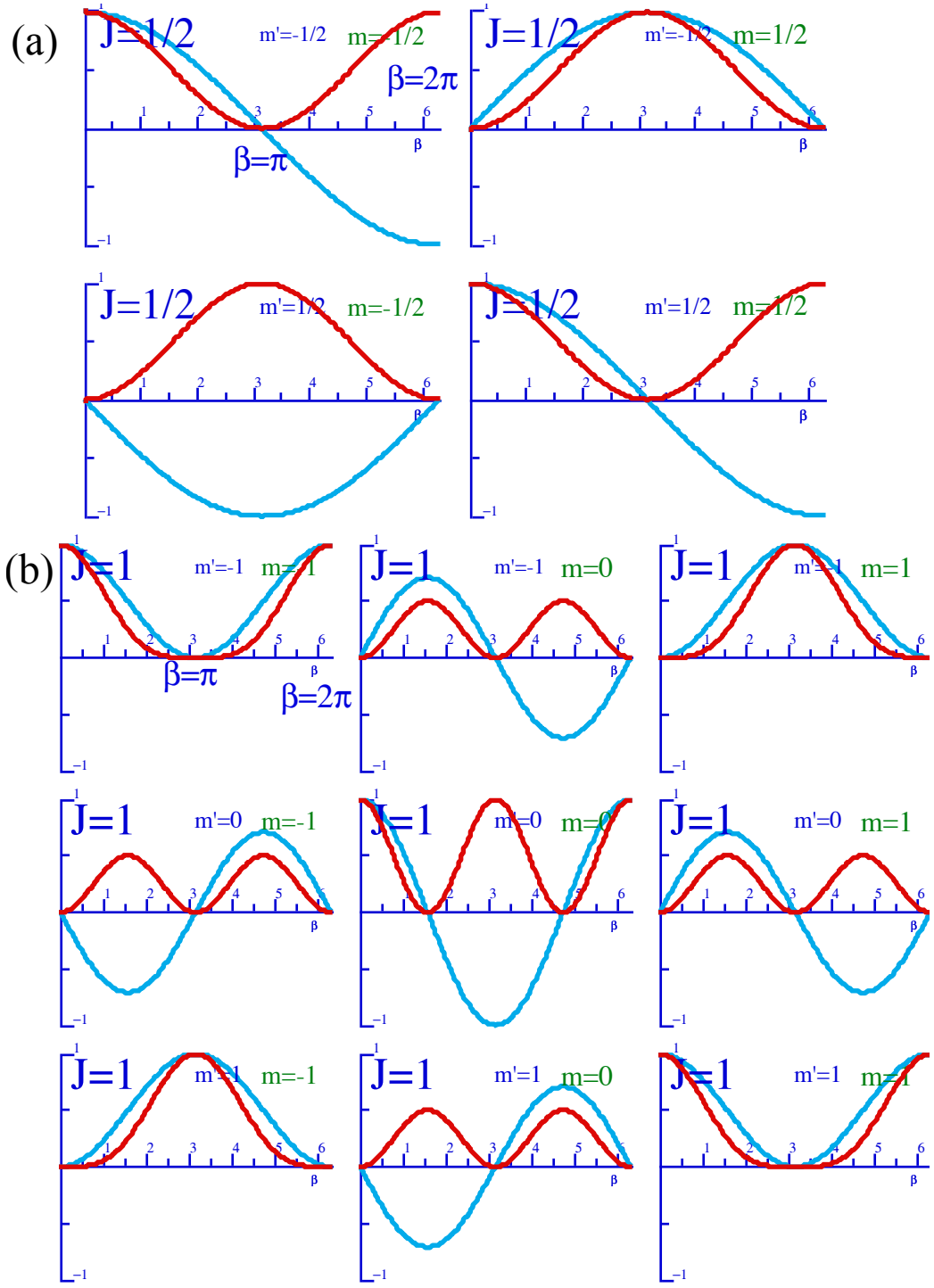

Fig. 23.2.3 b-Plots of D-amplitude and probability for (a) j=1/2, and (b) j=1.

(b) Molecular rotors: a quantum coordinate frame

The application (23.1.17) of *D*-matrix functions as molecular wavefunctions is a beautiful example of symmetry analysis and a *quantum frame*. The molecule has a body-frame but is usually quite uncertain how it is oriented in the lab frame in a rotor state of definite lab-*z*-value *m* and body-*z*-value *n* as for

$$\left|{}^{j}_{m,n}\right\rangle=\frac{1}{N}\int d(\alpha\beta\gamma)D^{j*}_{m,n}(\alpha\beta\gamma)\sqrt{\ell^j}\,|\alpha\beta\gamma\rangle\,. \qquad (23.2.4a)$$

(Recall (23.1.18).) The probability amplitude $D^{j*}_{mn}(\alpha,\beta,\gamma)$ for finding the rotor at Euler position (α,β,γ) is quite "fuzzy" usually, only for the higher *j, m,* and *n*-quanta does it "sharpen up" noticeably.

To help visualize the situation we shall plot its $D^{j}_{mn}(0,\beta,0)$ waves using to the geometry of its angular-momentum uncertainty cones as in Fig. 23.2.4. In so doing, we are ignoring the plane wave phase factors associated with the total wavefunction around the lab α-azimuth and the body γ-azimuth.

$$\langle\alpha\beta\gamma\left|{}^{j}_{m,n}\right\rangle=D^{j*}_{m,n}(\alpha\beta\gamma)\sqrt{2j+1}=e^{im\alpha}D^{j*}_{m,n}(0\beta0)e^{in\gamma}\sqrt{2j+1}\,. \qquad (23.2.4b)$$

These are needed to get proper time behavior, but they do not affect pure-state probability distributions.

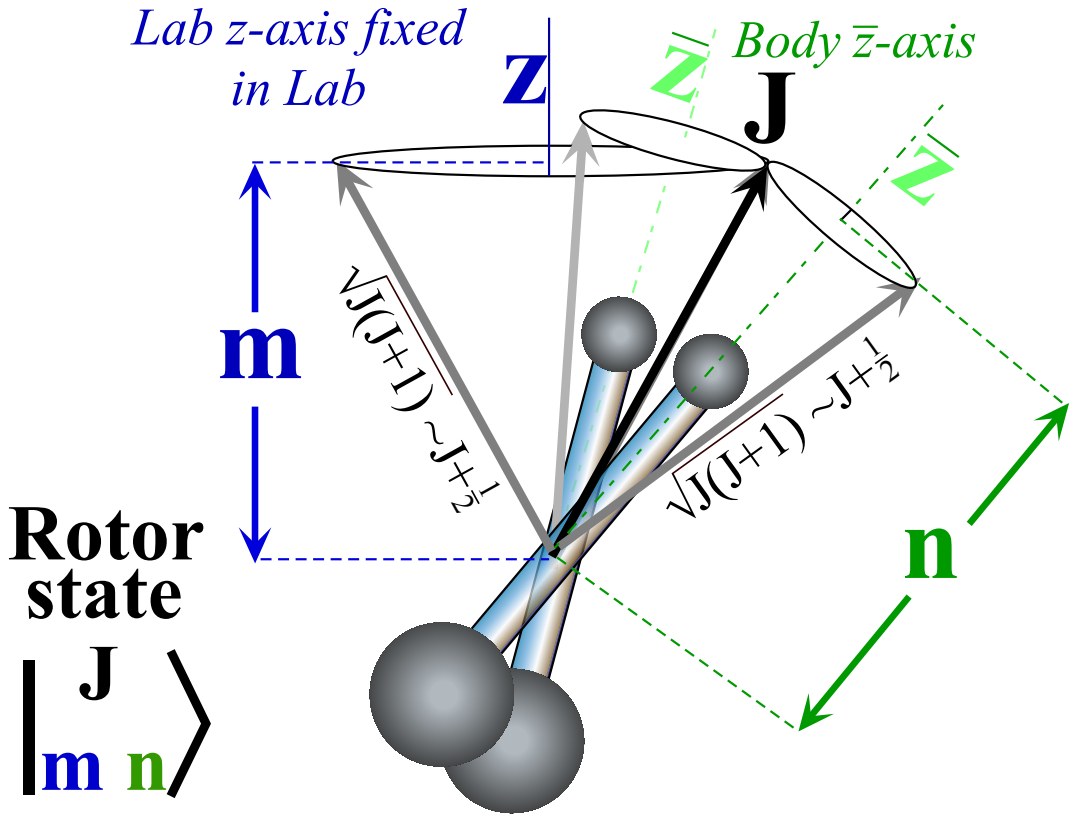

Fig. 23.2.4 Lab view of rotor in definite j, m, and n-quantum state.

The Fig. 23.2.4 shows schematically the range of motion permitted by the demands of angular quantization with definite values for J=*j, m,* and *n*-quanta. The **J**-vector can swivel around its lab-fixed cone of altitude *m* while it simultaneously swivels about the body-fixed cone of altitude *n*. However, in the lab frame, the body is doing its share of swiveling, too. This reflected in the *D*-distributions shown for *j=2* in Fig. 23.2.5. The second column *D*-plots are the same as those in Fig. 23.2.1.

While it is tempting, we cannot equate the lab and body J-cones with the classical ω-cones. The latter relate to angular velocity ω, which is classically related to momentum **J=I•ω** by inertia tensor **I**.

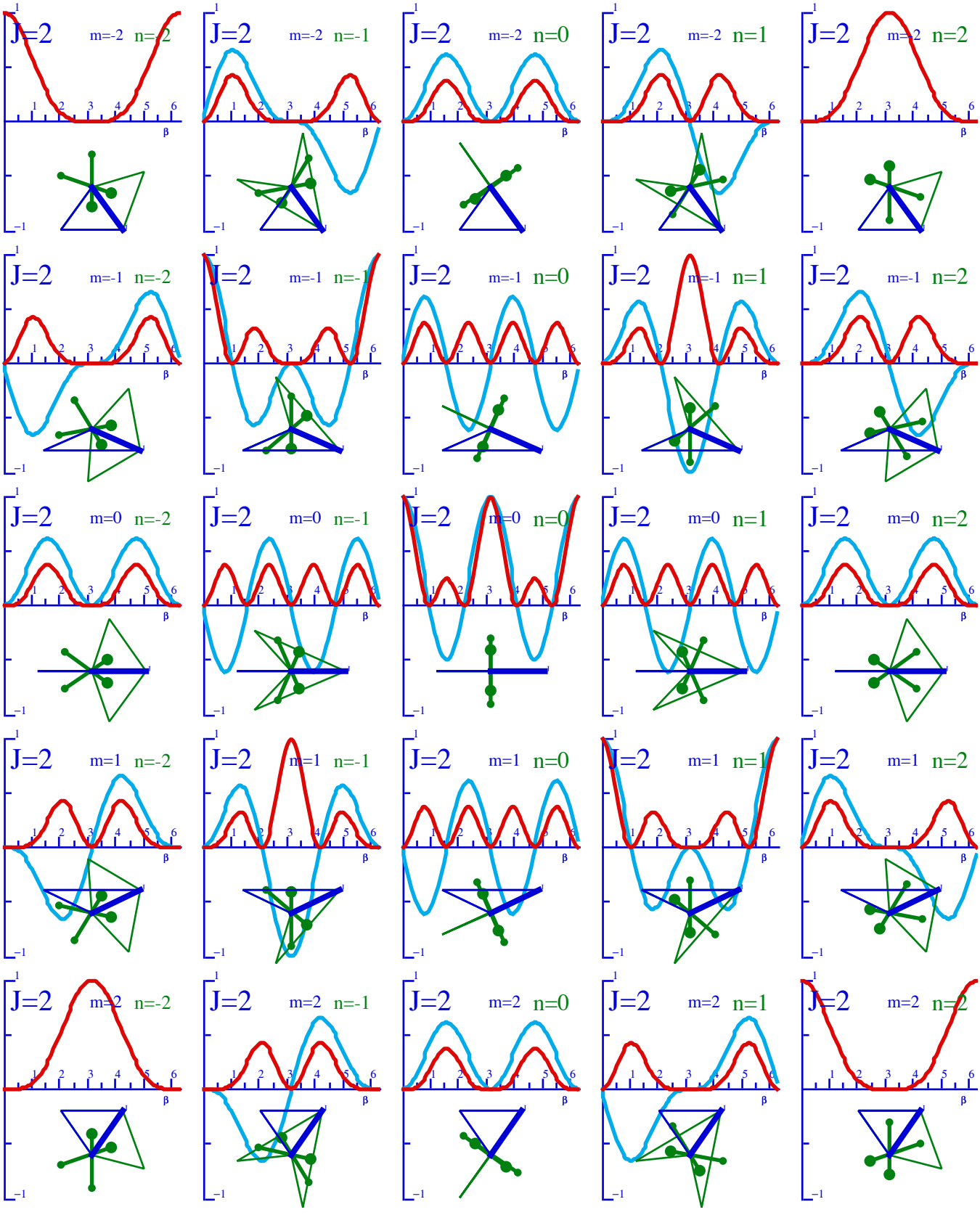

Fig. 23.2.5 Lab views of rotor cones and wave distributions in definite j=2, m, and n-quantum states.

The distribution widths are consistent with the swivel angles allowed by the angular momentum cones, which for *j=2* are at least a radian or two. To obtain a more precisely peaked distributions it is necessary to make all three quantum numbers as high as possible. Some examples with ten times the momentum, or *j=20*, are shown in Fig. 23.2.6. The highest *m* and *n* values have narrow *D*-distributions.

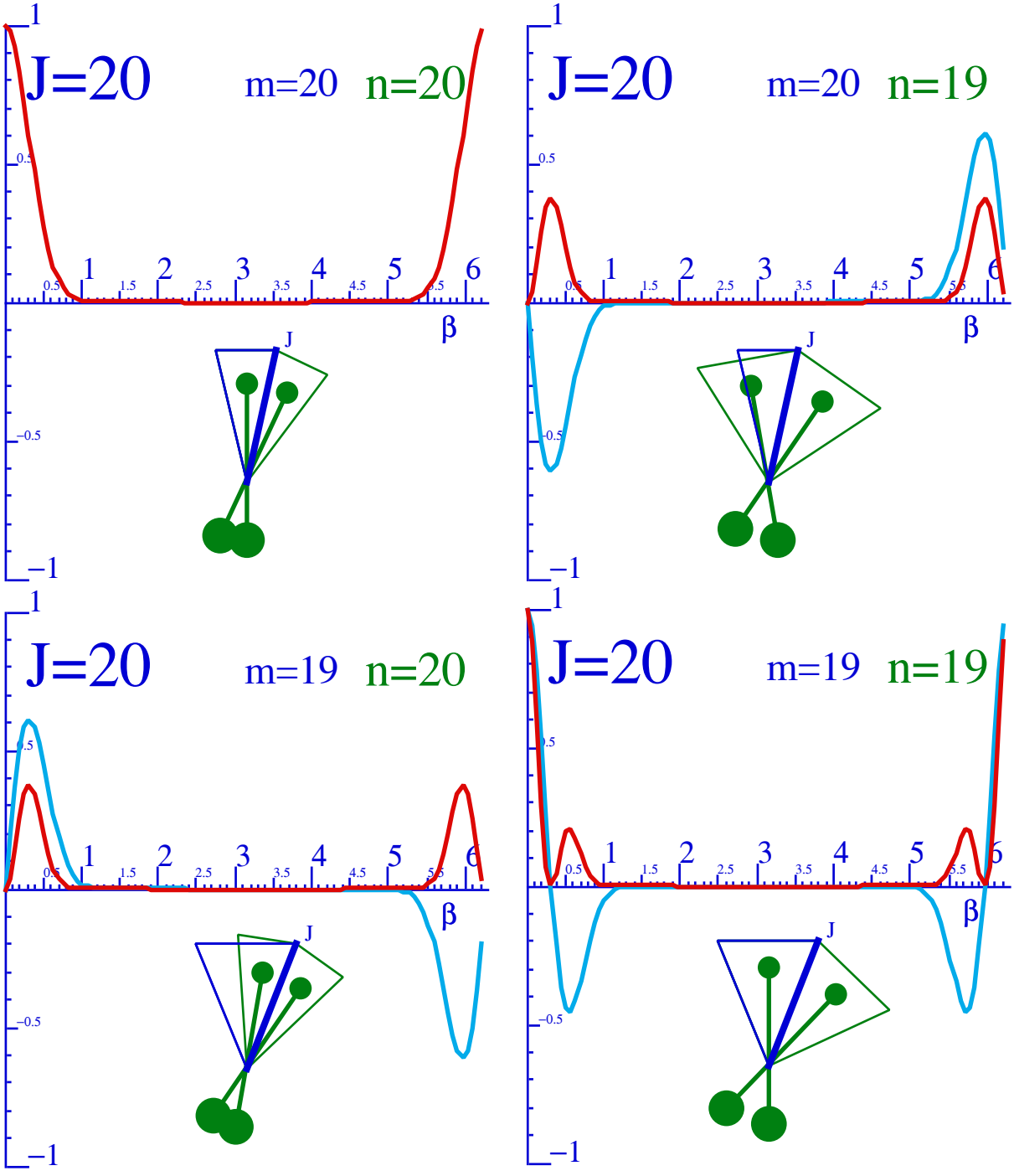

Fig. 23.2.6 Lab view of rotor in definite j=20, and upper m, and n-quantum states.

Narrow bi-modal or two-peak distributions occur for the same high *j* and *m* but with *n=0* as shown by examples in Fig. 23.2.7. For a prolate molecular rotor (long and narrow like the one sketched in preceding

figures) the low-*n* states have the lowest energy levels of a given *j*. (Recall Fig. 23.1.3(b).) Narrow bodies require huge kinetic energy in order to achieve a given angular momentum along their narrow bodies so high-n means high energy. A diatomic molecule made of two point particles would require infinite energy to achieve even *n=1*. The same holds for a single orbiting particle, so the *n=0* states are their only option. Each *(j, n=0)*-state has 2j+1 different m-values *(m = -j, -j+1,..., j-1, j)*, which for a free-rotation belong to a *(2j+1)*-fold degenerate rotational energy level.

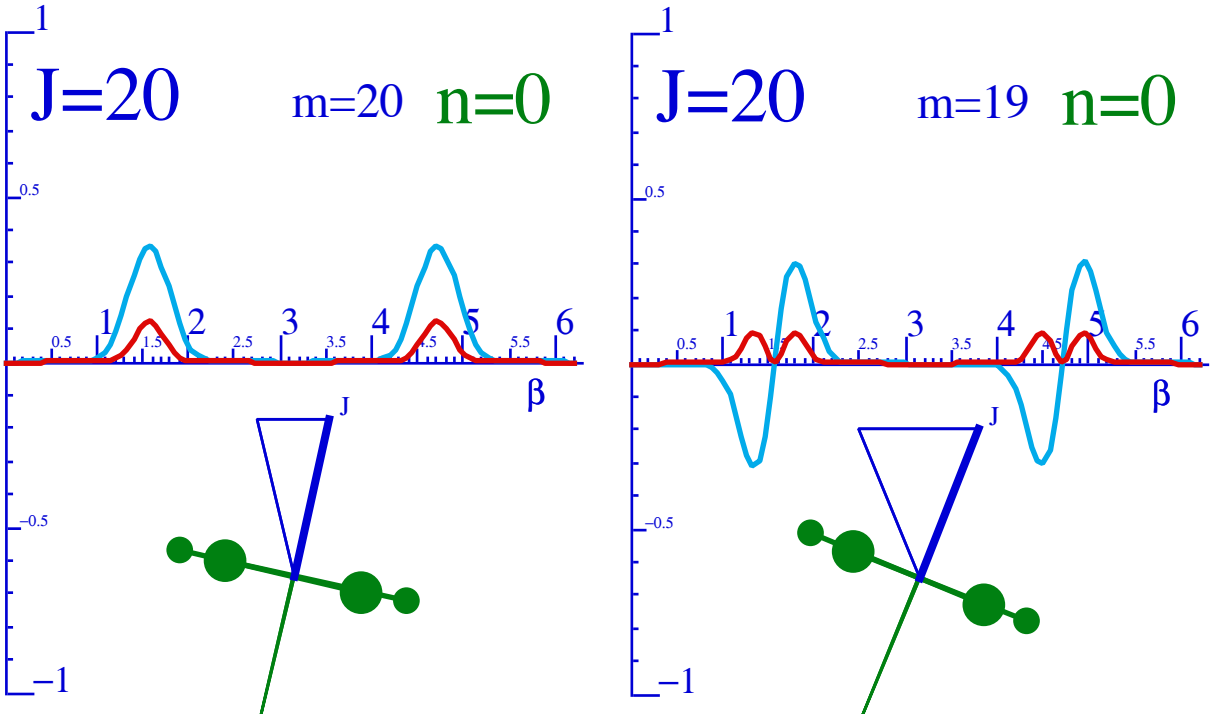

Fig. 23.2.7 Lab view of rotor in definite j=20, and upper m, but (n=0)-quantum states.

We now turn our attention to some of the properties of such orbital levels and study orbital wavefunctions useful in the study of electronic structure of atoms and molecules.

23.3 Orbital Wave-Functions

We now examine wavefunctions of point-like bodies such as electrons or line-like bodies such as diatomic molecules whose bodies have no bodies! Like high-fashion models, their Z-body axial inertia is zero, or in the case of nuclear rotors, near-zero. This means the A-parameter in (23.1.21) is infinite or, for nuclei, some millions of Volts. So, non-zero n-quanta have huge energy. Energetically allowed energy waves are just the center ($n=0$) column of the D^j-matrices. (Half-integral j have no ($n=0$) states.)

(a) (j=1) 3-Vector or dipole waves and transformations

For $j=1$ the center column of (23.1.15a) has three functions which make a complex unit 3-vector.

$$\begin{aligned}
\sqrt{4\pi/3}\,Y^{\ell=1}_{m=1}(\phi\theta) &= D^{1*}_{1,0}(\phi\theta 0) = -e^{i\phi}\frac{\sin\theta}{\sqrt{2}}\\
\sqrt{4\pi/3}\,Y^{\ell=1}_{m=0}(\phi\theta) &= D^{1*}_{0,0}(\phi\theta 0) = \cos\theta\\
\sqrt{4\pi/3}\,Y^{\ell=1}_{m=-1}(\phi\theta) &= D^{1*}_{-1,0}(\phi\theta 0) = e^{-i\phi}\frac{\sin\theta}{\sqrt{2}}
\end{aligned} \qquad (23.3.1)$$

This is seen by converting the Euler spherical polar coordinates to Cartesian unit vector coordinates.

$$x/r = \cos\phi\sin\theta\ ,\ \ y/r = \sin\phi\sin\theta\ \ ,\ \ z/r = \cos\theta \qquad (23.3.2)$$

A 3-vector begins to emerge.

$$\begin{aligned}
D^{1*}_{1,0}(\phi\theta 0) &= -e^{i\phi}\frac{\sin\theta}{\sqrt{2}} = -\frac{\cos\phi\sin\theta + i\cos\phi\sin\theta}{\sqrt{2}} = -\frac{x+iy}{r\sqrt{2}}\\
D^{1*}_{0,0}(\phi\theta 0) &= \cos\theta \quad = \quad \cos\theta \quad = z/r\\
D^{1*}_{-1,0}(\phi\theta 0) &= e^{-i\phi}\frac{\sin\theta}{\sqrt{2}} = \frac{\cos\phi\sin\theta - i\cos\phi\sin\theta}{\sqrt{2}} = \frac{x-iy}{r\sqrt{2}}
\end{aligned} \qquad (23.3.3)$$

The two components involving x and y have the complex circular polarization form $(x\pm iy)$. It is tempting to view this as a coordinate transformation from real Cartesian $\{x,y,z\}$. But, we must resist temptation to deviate from our rule of always defining base vectors first before coordinates. We define a base state relation based on (23.3.3). (It is just writing moving-wave states in terms of standing-wave bases.)

$$\begin{aligned}
\left|{}^{1}_{1}\right\rangle &= \frac{-1}{\sqrt{2}}\left|{}^{1}_{x}\right\rangle - \frac{i}{\sqrt{2}}\left|{}^{1}_{y}\right\rangle\\
\left|{}^{1}_{0}\right\rangle &= \left|{}^{1}_{z}\right\rangle\\
\left|{}^{1}_{-1}\right\rangle &= \frac{1}{\sqrt{2}}\left|{}^{1}_{x}\right\rangle - \frac{i}{\sqrt{2}}\left|{}^{1}_{y}\right\rangle
\end{aligned} \qquad (23.3.4a) \qquad \begin{pmatrix} \left\langle {}^{1}_{x}\middle|{}^{1}_{1}\right\rangle & \left\langle {}^{1}_{x}\middle|{}^{1}_{0}\right\rangle & \left\langle {}^{1}_{x}\middle|{}^{1}_{-1}\right\rangle \\ \left\langle {}^{1}_{y}\middle|{}^{1}_{1}\right\rangle & \left\langle {}^{1}_{y}\middle|{}^{1}_{0}\right\rangle & \left\langle {}^{1}_{y}\middle|{}^{1}_{-1}\right\rangle \\ \left\langle {}^{1}_{z}\middle|{}^{1}_{1}\right\rangle & \left\langle {}^{1}_{z}\middle|{}^{1}_{0}\right\rangle & \left\langle {}^{1}_{z}\middle|{}^{1}_{-1}\right\rangle \end{pmatrix} = \begin{pmatrix} -\frac{1}{\sqrt{2}} & 0 & \frac{1}{\sqrt{2}} \\ -\frac{i}{\sqrt{2}} & 0 & -\frac{i}{\sqrt{2}} \\ 0 & 1 & 0 \end{pmatrix}$$

The inverse (†) of (23.3.4a) is the *3-dimensional linear-to-circular polarization transformation matrix*.

$$\begin{pmatrix} \left\langle {}^{1}_{1}\middle|{}^{1}_{x}\right\rangle & \left\langle {}^{1}_{1}\middle|{}^{1}_{y}\right\rangle & \left\langle {}^{1}_{-1}\middle|{}^{1}_{z}\right\rangle \\ \left\langle {}^{1}_{0}\middle|{}^{1}_{x}\right\rangle & \left\langle {}^{1}_{0}\middle|{}^{1}_{y}\right\rangle & \left\langle {}^{1}_{0}\middle|{}^{1}_{z}\right\rangle \\ \left\langle {}^{1}_{-1}\middle|{}^{1}_{x}\right\rangle & \left\langle {}^{1}_{-1}\middle|{}^{1}_{y}\right\rangle & \left\langle {}^{1}_{-1}\middle|{}^{1}_{z}\right\rangle \end{pmatrix} = \begin{pmatrix} -\frac{1}{\sqrt{2}} & \frac{i}{\sqrt{2}} & 0 \\ 0 & 0 & 1 \\ \frac{1}{\sqrt{2}} & \frac{i}{\sqrt{2}} & 0 \end{pmatrix} \qquad (23.3.4b)$$

Applying the circular-to-linear transformation of the D^1 matrices yields familiar real rotation matrices.

$$\begin{pmatrix} \left\langle \begin{smallmatrix}1\\x\end{smallmatrix}\middle|\begin{smallmatrix}1\\1\end{smallmatrix}\right\rangle & \left\langle \begin{smallmatrix}1\\x\end{smallmatrix}\middle|\begin{smallmatrix}1\\0\end{smallmatrix}\right\rangle & \left\langle \begin{smallmatrix}1\\x\end{smallmatrix}\middle|\begin{smallmatrix}1\\-1\end{smallmatrix}\right\rangle \\ \left\langle \begin{smallmatrix}1\\y\end{smallmatrix}\middle|\begin{smallmatrix}1\\1\end{smallmatrix}\right\rangle & \left\langle \begin{smallmatrix}1\\y\end{smallmatrix}\middle|\begin{smallmatrix}1\\0\end{smallmatrix}\right\rangle & \left\langle \begin{smallmatrix}1\\y\end{smallmatrix}\middle|\begin{smallmatrix}1\\-1\end{smallmatrix}\right\rangle \\ \left\langle \begin{smallmatrix}1\\z\end{smallmatrix}\middle|\begin{smallmatrix}1\\1\end{smallmatrix}\right\rangle & \left\langle \begin{smallmatrix}1\\z\end{smallmatrix}\middle|\begin{smallmatrix}1\\0\end{smallmatrix}\right\rangle & \left\langle \begin{smallmatrix}1\\z\end{smallmatrix}\middle|\begin{smallmatrix}1\\-1\end{smallmatrix}\right\rangle \end{pmatrix} \cdot \begin{pmatrix} D^1_{1,1}(\alpha\beta\gamma) & D^1_{1,0} & D^1_{1,-1} \\ D^1_{0,1} & D^1_{0,0} & D^1_{0,-1} \\ D^1_{-1,1} & D^1_{-1,0} & D^1_{-1,-1} \end{pmatrix} \cdot \begin{pmatrix} \left\langle \begin{smallmatrix}1\\1\end{smallmatrix}\middle|\begin{smallmatrix}1\\x\end{smallmatrix}\right\rangle & \left\langle \begin{smallmatrix}1\\1\end{smallmatrix}\middle|\begin{smallmatrix}1\\y\end{smallmatrix}\right\rangle & \left\langle \begin{smallmatrix}1\\-1\end{smallmatrix}\middle|\begin{smallmatrix}1\\z\end{smallmatrix}\right\rangle \\ \left\langle \begin{smallmatrix}1\\0\end{smallmatrix}\middle|\begin{smallmatrix}1\\x\end{smallmatrix}\right\rangle & \left\langle \begin{smallmatrix}1\\0\end{smallmatrix}\middle|\begin{smallmatrix}1\\y\end{smallmatrix}\right\rangle & \left\langle \begin{smallmatrix}1\\0\end{smallmatrix}\middle|\begin{smallmatrix}1\\z\end{smallmatrix}\right\rangle \\ \left\langle \begin{smallmatrix}1\\-1\end{smallmatrix}\middle|\begin{smallmatrix}1\\x\end{smallmatrix}\right\rangle & \left\langle \begin{smallmatrix}1\\-1\end{smallmatrix}\middle|\begin{smallmatrix}1\\y\end{smallmatrix}\right\rangle & \left\langle \begin{smallmatrix}1\\-1\end{smallmatrix}\middle|\begin{smallmatrix}1\\z\end{smallmatrix}\right\rangle \end{pmatrix} = \begin{pmatrix} D^1_{x,x}(\alpha\beta\gamma) & D^1_{x,y} & D^1_{x,z} \\ D^1_{y,x} & D^1_{y,y} & D^1_{y,z} \\ D^1_{z,x} & D^1_{z,y} & D^1_{z,z} \end{pmatrix}$$

For example the Euler β-rotation around the *Y*-axis is just exactly that. (23.3.5a)

$$\begin{pmatrix} -\frac{1}{\sqrt2} & 0 & \frac{1}{\sqrt2} \\ -\frac{i}{\sqrt2} & 0 & -\frac{i}{\sqrt2} \\ 0 & 1 & 0 \end{pmatrix} \cdot \begin{pmatrix} \frac{1+\cos\beta}{2} & \frac{-\sin\beta}{\sqrt2} & \frac{1-\cos\beta}{2} \\ \frac{\sin\beta}{\sqrt2} & \cos\beta & \frac{-\sin\beta}{\sqrt2} \\ \frac{1-\cos\beta}{2} & \frac{\sin\beta}{\sqrt2} & \frac{1+\cos\beta}{2} \end{pmatrix} \cdot \begin{pmatrix} -\frac{1}{\sqrt2} & \frac{i}{\sqrt2} & 0 \\ 0 & 0 & 1 \\ \frac{1}{\sqrt2} & \frac{i}{\sqrt2} & 0 \end{pmatrix} = \begin{pmatrix} \cos\beta & 0 & \sin\beta \\ 0 & 1 & 0 \\ -\sin\beta & 0 & \sin\beta \end{pmatrix} \qquad (23.3.5b)$$

The Euler α-rotation around the *Z*-axis is in the correct direction, too.

$$\begin{pmatrix} -\frac{1}{\sqrt2} & 0 & \frac{1}{\sqrt2} \\ -\frac{i}{\sqrt2} & 0 & -\frac{i}{\sqrt2} \\ 0 & 1 & 0 \end{pmatrix} \cdot \begin{pmatrix} e^{-i\alpha} & \cdot & \cdot \\ \cdot & 1 & \cdot \\ \cdot & \cdot & e^{i\alpha} \end{pmatrix} \cdot \begin{pmatrix} -\frac{1}{\sqrt2} & \frac{i}{\sqrt2} & 0 \\ 0 & 0 & 1 \\ \frac{1}{\sqrt2} & \frac{i}{\sqrt2} & 0 \end{pmatrix} = \begin{pmatrix} \cos\alpha & -\sin\alpha & 0 \\ \sin\alpha & \cos\alpha & 0 \\ 0 & 0 & 1 \end{pmatrix} \qquad (23.3.5c)$$

Combining these gives the real vector Euler rotation first derived in (10.A.6b).

$$\begin{pmatrix} D^1_{x,x}(\alpha\beta\gamma) & D^1_{x,y} & D^1_{x,z} \\ D^1_{y,x} & D^1_{y,y} & D^1_{y,z} \\ D^1_{z,x} & D^1_{z,y} & D^1_{z,z} \end{pmatrix} = \begin{pmatrix} \cos\alpha\cos\beta\cos\gamma - \sin\alpha\sin\gamma & -\cos\alpha\cos\beta\sin\gamma - \sin\alpha\cos\gamma & \cos\alpha\sin\beta \\ \sin\alpha\cos\beta\cos\gamma + \cos\alpha\sin\gamma & -\sin\alpha\cos\beta\sin\gamma + \cos\alpha\cos\gamma & \sin\alpha\sin\beta \\ -\cos\gamma\sin\beta & \sin\gamma\sin\beta & \cos\beta \end{pmatrix} \qquad (23.3.5d)$$

The only finite energy waves for a diatomic molecule (or a point particle in a spherical potential) are the three functions in the last *(z)* column of the *D*-matrix (23.1.20a). (This is now the (*n=0*)-column.)

$$\begin{aligned} \Psi^1_x(\phi,\theta) = D^1_{x,z}(\phi,\theta,0), \quad \Psi^1_y(\phi,\theta) = D^1_{y,z}(\phi,\theta,0), \quad \Psi^1_z(\phi,\theta) &= D^1_{z,z}(\phi,\theta,0) \\ = \cos\phi\sin\theta, \qquad = \sin\phi\sin\theta, \qquad = \cos\theta. \end{aligned} \qquad (23.3.6a)$$

Plotting angular three-dimensional wavefunctions is tricky, and there are many ways to do it. In Fig. 23.3.1 is a plot of the three wave functions done by simply setting $r=\Psi(\phi\theta)$. Each plot is two kissing spheres lined up along the *x*, *y*, or *z* axes with one representing a (+) phase and the other a (-) phase. One idea conveyed by this plot is the electric dipole-vector geometry of the *j=1* waves. Indeed, it resembles the wave amplitude pattern of a dipole antenna. Other names for these waves are *"p-orbitals"* where *p* stands for "principal" lines in H-spectra. (This ancient notation doesn't tell you much about the shape of the waves.) They are called *vector ligands* (meaning "fingers") or *π-bonds* in chemistry , and are important for holding our molecules together. By taking any linear combination

$$\begin{aligned} \Psi^1_{ABC}(\phi,\theta) &= A\Psi^1_x(\phi,\theta) + B\Psi^1_y(\phi,\theta) + C\Psi^1_z(\phi,\theta) \\ &= A\cos\phi\sin\theta + B\sin\phi\sin\theta + C\cos\theta. \end{aligned} \qquad (23.3.6b)$$

it is possible to point the "finger" in any direction *(A, B, C)* in Cartesian 3-space.

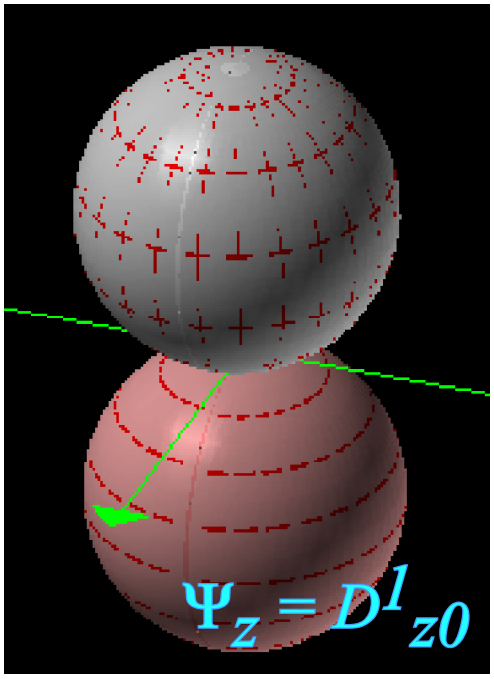

j = 1
Standing
p-Waves

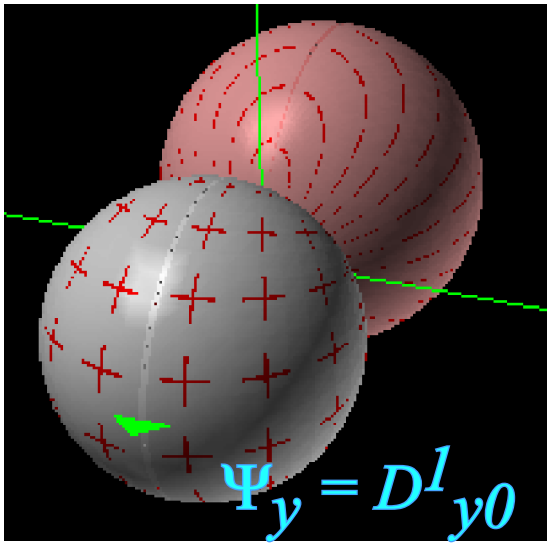

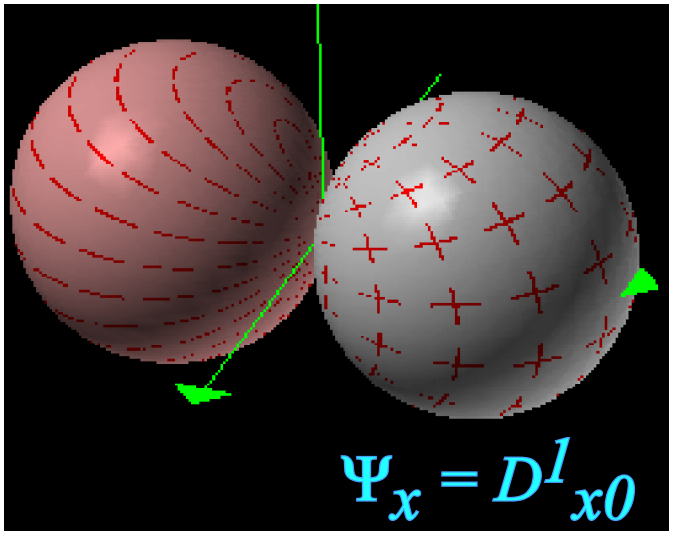

23.3.1 Point particle or dipole rotor p-waves for triplet j= 1..(Only rotor n=0 allowed).

As long as there is no potential field around to split this triply degenerate set, we are allowed to mix them arbitrarily and still have an eigenstate. Making them back into the moving-wave spherical harmonics is certainly an option. Mixing the *x*- and i*y*-ligands gives moving waves in the *xy*-plane. Ψ_0 is unaltered.

$$\begin{aligned} \Psi^1_1(\phi,\theta) &= D^{1*}_{1,0}(\phi,\theta,0), & \Psi^1_{-1}(\phi,\theta) &= D^{1*}_{-1,0}(\phi,\theta,0), & \Psi^1_0(\phi,\theta) &= D^{1*}_{0,0}(\phi,\theta,0) \\ &= -e^{i\phi}\sin\theta/\sqrt{2}, & &= e^{-i\phi}\sin\theta/\sqrt{2}, & &= \cos\theta. \end{aligned} \qquad (23.3.6c)$$

Degenerate probability distributions $|X^1{}_{\pm 1}|^2$ don't move unless some *j=0* or other energy state is added. But, the $|X^1{}_{\pm 1}|^2$ are symmetric in the *xy*-plane as shown in Fig. 23.3.2. (Recall Fig. 4.6.5, too.)

$|\Psi_x|^2 = |D^1_{x0}|^2$

$|\Psi_y|^2 = |D^1_{y0}|^2$

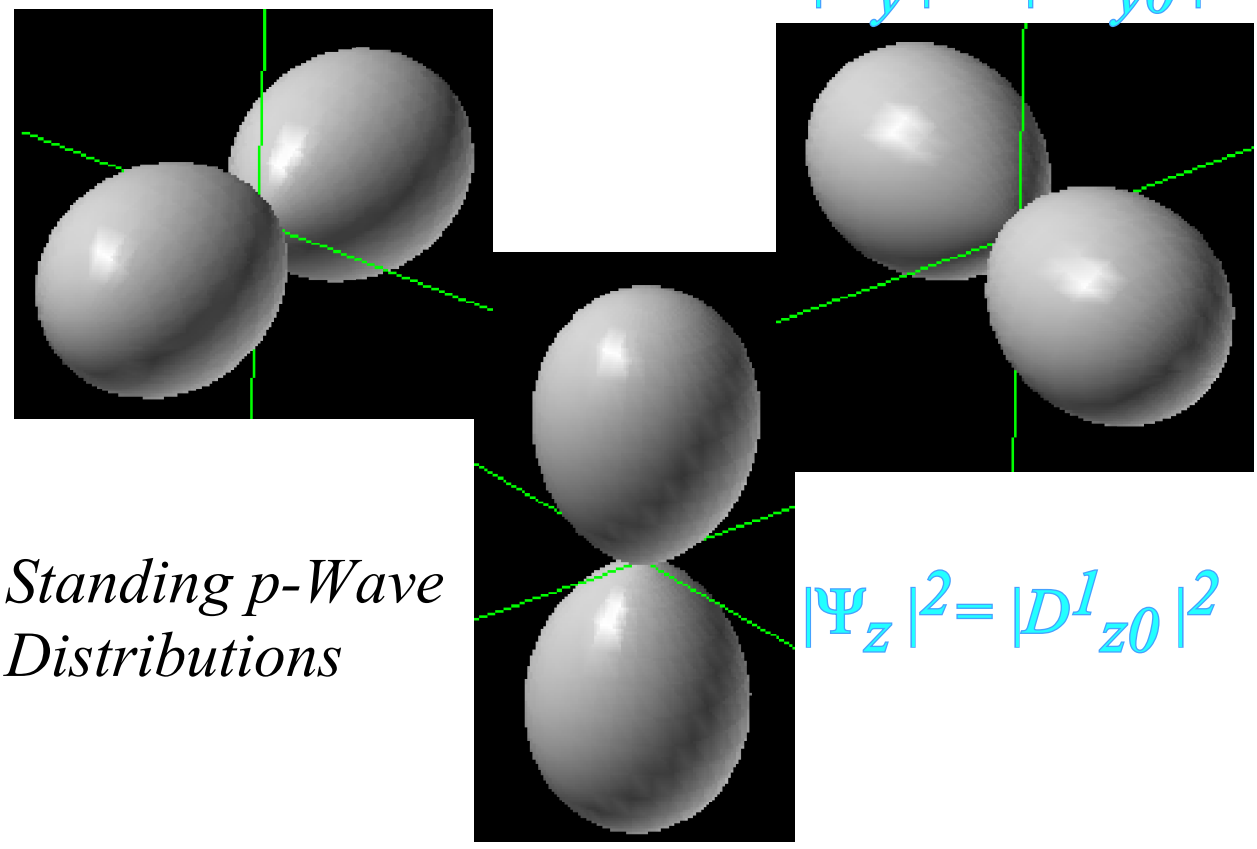

Standing p-Wave Distributions

$|\Psi_z|^2 = |D^1_{z0}|^2$

Moving p-Wave Distributions

$|\Psi_{-1}|^2 = |D^1_{-10}|^2$

$|\Psi_1|^2 = |D^1_{10}|^2$

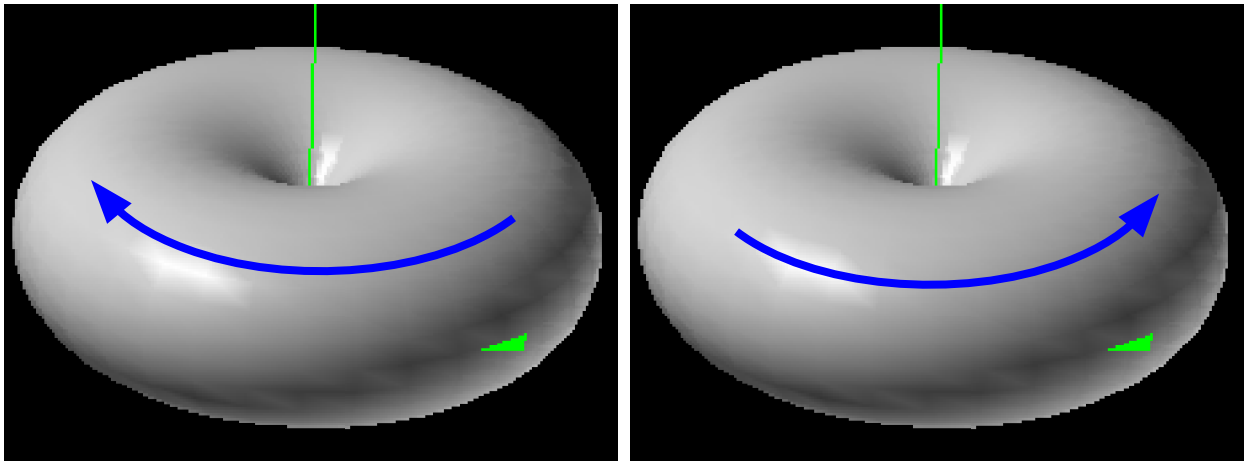

23.3.2 Point particle or dipole rotor (j=1) probability distribution for standing and moving waves.

(b) (j=2) Tensor or quadrupole waves

R(3) rotational states of two quanta *(j=2)* correspond to *SU(2)* oscillator states with four *(υ=4)* quanta. Both the diatomic rotor (for which *n=0*) and an orbiting point particle have the same *(j=2)* quantum state degeneracy with five substates. The five moving-wave functions or spherical harmonics are from the center *(n=0)* column of the conjugated D^{2}-matrix (23.1.15d)

$$\begin{aligned}
\sqrt{4\pi/5}\,Y^{\ell=2}_{m=2}(\phi\theta) &= D^{2*}_{2,0}(\phi\theta 0) = \sqrt{\frac{3}{8}}e^{i2\phi}\sin^2\theta &&= \sqrt{\frac{3}{8}}\frac{(x+iy)^2}{r^2}\\
\sqrt{4\pi/5}\,Y^{\ell=2}_{m=1}(\phi\theta) &= D^{2*}_{1,0}(\phi\theta 0) = -\sqrt{\frac{3}{2}}e^{i\phi}\sin\theta\cos\theta &&= -\sqrt{\frac{3}{2}}\frac{(x+iy)z}{r^2}\\
\sqrt{4\pi/5}\,Y^{\ell=2}_{m=0}(\phi\theta) &= D^{2*}_{0,0}(\phi\theta 0) = \frac{3\cos^2\theta-1}{2} &&= \frac{3z^2-r^2}{2r^2}\\
\sqrt{4\pi/5}\,Y^{\ell=2}_{m=-1}(\phi\theta) &= D^{2*}_{-1,0}(\phi\theta 0) = \sqrt{\frac{3}{2}}e^{-i\phi}\sin\theta\cos\theta &&= \sqrt{\frac{3}{2}}\frac{(x-iy)z}{r^2}\\
\sqrt{4\pi/5}\,Y^{\ell=2}_{m=-2}(\phi\theta) &= D^{2*}_{-2,0}(\phi\theta 0) = \sqrt{\frac{3}{8}}e^{-i2\phi}\sin^2\theta &&= \sqrt{\frac{3}{8}}\frac{(x-iy)^2}{r^2}
\end{aligned} \qquad (23.3.7)$$

Spherical *2^k-multipole functions X^k_q* or *X-functions* are *Y*-functions times the *k*-th power of radius *(r^k)*.

$$X^k_q = r^k D^{k*}_{q,0} = \sqrt{\frac{4\pi}{2k+1}}r^k Y^k_q \qquad (23.3.8)$$

The *(k=2) X*-functions or *quadrupole functions X^2_q* are complex quadratic polynomials of *x, y*, and *z*.

$$\begin{aligned}
X^2_{\pm 2} &= \sqrt{\frac{3}{8}}(x\pm iy)^2 = \sqrt{\frac{3}{8}}\left(x^2-y^2\pm i2xy\right)^2\\
X^2_{\pm 1} &= \mp\sqrt{\frac{3}{2}}(x\pm iy)z = \sqrt{\frac{3}{8}}\left(\mp xz+iyz\right)^2\\
X^2_0 &= \frac{1}{2}\left(3z^2-r^2\right) = \frac{1}{2}\left(2z^2-x^2-y^2\right)
\end{aligned} \qquad (23.3.9a)$$

The real and imaginary parts of the X^2_q are the standing-wave eigenfunctions of total angular momentum *(j=2)* but zero expected *z*-component momentum.($\langle \mathbf{J}_Z\rangle=0$) Standing waves are plotted in Fig. 23.3.3.

$$\begin{aligned}
&\left(X^2_{+2}+X^2_{-2}\right)/\sqrt{2} = \sqrt{3}\left(x^2-y^2\right)/2\,, \quad &&\left(X^2_{+2}-X^2_{-2}\right)/\sqrt{2} = i\sqrt{3}(xy),\\
&\left(X^2_{+1}+X^2_{-1}\right)/\sqrt{2} = i\sqrt{3}(yz)\,, &&\left(X^2_{+1}-X^2_{-1}\right)/\sqrt{2} = \sqrt{3}(xz).
\end{aligned} \qquad (23.3.9b)$$

Wave crests (+) and troughs (-) are shown. The corresponding moving-wave distributions are shown below for magnetic quanta *m = 2, 1*, and *0*. The last case $|X^2_0|^2$ is the distribution of the wave

$$X^2_0 = \frac{1}{2}\left(2z^2-x^2-y^2\right) = r^2P_2(\cos\theta) \qquad (23.3.9c)$$

which is <u>not</u> moving. X^2_0 is the only wave of the five that has zero current or momentum *(m=0)*, and it represents the only state with non-zero probability on the *z*-axis and the only one of the five that has a cylindrically symmetric wavefunction X^2_0 . Its probability function $|X^2_0|^2$ is symmetric, too, as are $|X^2_{\pm 1}|^2$ and $|X^2_{\pm 2}|^2$, but $X^2_{\pm 1}$ is a ±-rotating X^2_{xz} or X^2_{yz} wave, and $X^2_{\pm 2}$ is a ±-rotating X^2_{xy} or $X^2_{x^2-y^2}$ wave.

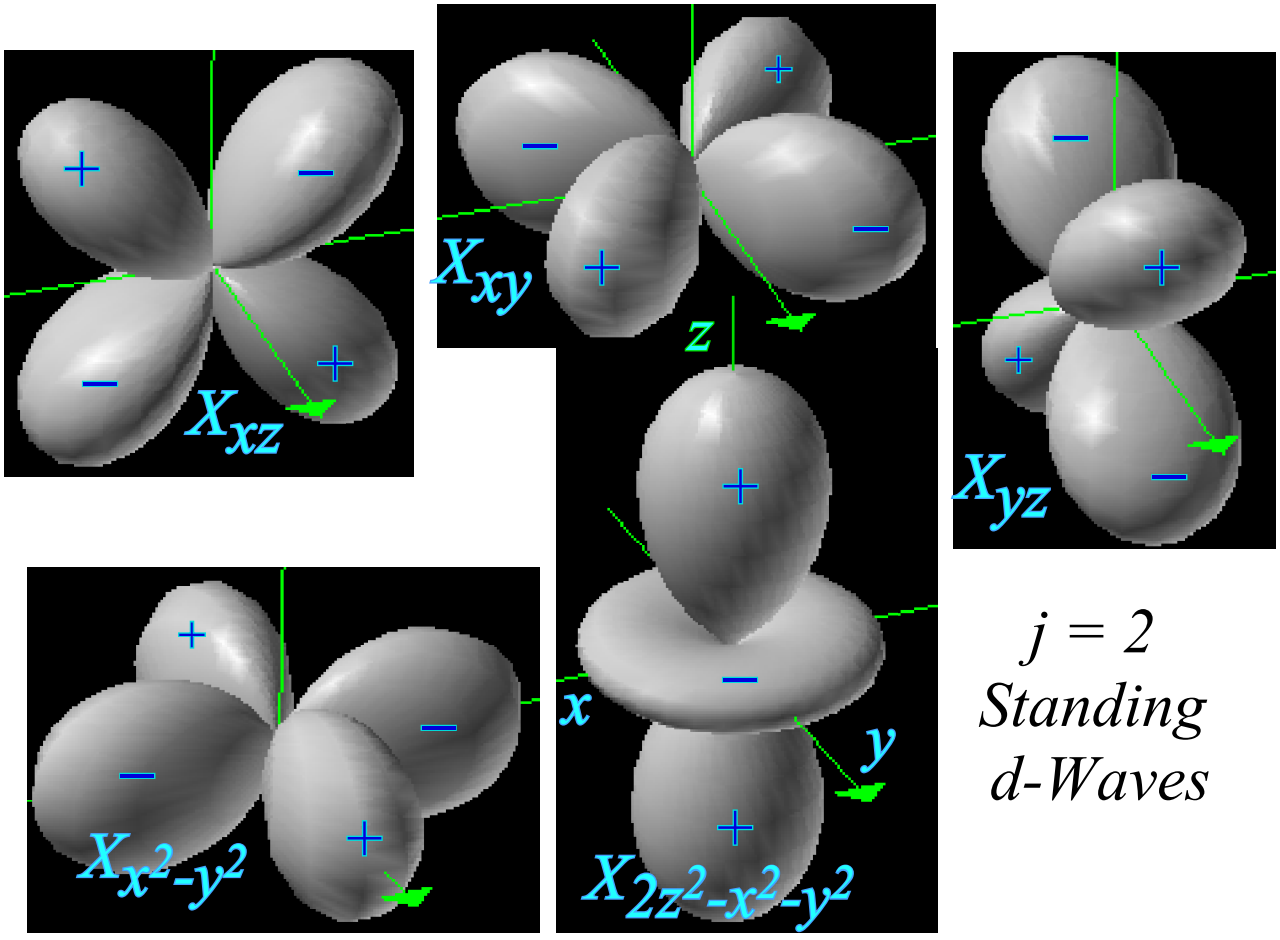

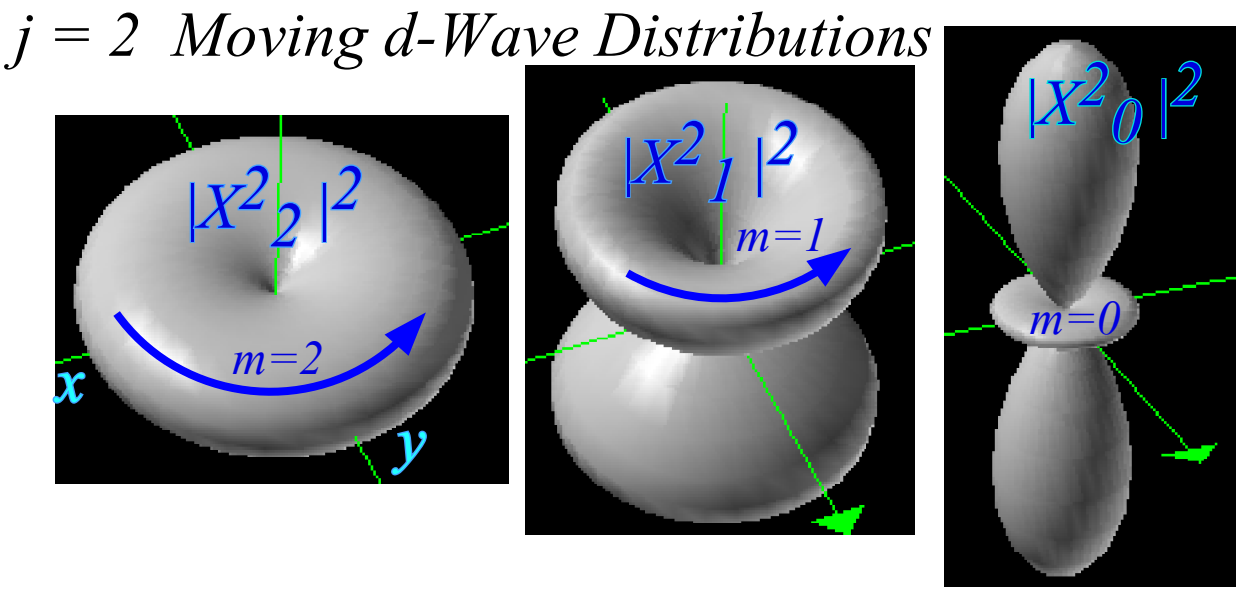

Fig. 23.3.3 (Upper)(j=2)Standing waves (Lower) Probability distributions for (j=2) moving waves.

(c) (j=ℓ) 2^ℓ-Pole Multipole potentials and waves

Zero azimuthal angular momentum *(m=0)*-orbital waves for any integral total momentum ℓ are expressed in terms of *Legendre polynomials* P_ℓ as follows.

$$X_0^\ell = r^\ell D_{0,0}^\ell(\cdot\,\theta\,\cdot) = r^\ell P_\ell(\cos\theta) \qquad (23.3.10)$$

The Legendre P_ℓ *(cos*θ*)* functions are a basis for *multipole waves* and angular potentials. They may be viewed as derivatives of the simple *monopole potential* field of a single charge.

$$V^{monopole}(r) = \frac{q}{r} = \frac{qP_0(\cos\theta)}{r} \qquad (23.3.11)$$

The *z*-derivative of *r* raised to a power is used below.

$$\frac{\partial}{\partial z}(r)^n = n(r)^{n-1}\frac{\partial}{\partial z}\sqrt{x^2+y^2+z^2} = n(r)^{n-2}z$$

A *z*-derivative of $V^{monopole}$ is equivalent to putting an (+)-charge infinitesimally below a (-)-charge, that is, V(z +dz)-V(z). We flip the sign so a (+) charge is above a (-)-charge as in Fig. 23.3.4.The resulting potential field is a *dipole potential*. Its angular dependence is the (ℓ=*1*) Legendre function.

$$V^{dipole}(r) = -\frac{\partial}{\partial z}V^{monopole}(r) = \frac{qz}{r^3} = \frac{q\cos\theta}{r^2} = \frac{qP_1(\cos\theta)}{r^2} \qquad (23.3.12)$$

Now imagine copying a dipole, but with opposite charges, and placing the copy Δ*z* above the original as shown in Fig. 23.3.4. For infinitesimal Δ*z*, this is the same as another *z*-derivative. A *z*-derivative of the dipole potential gives the *quadrupole potential* with angular dependence of the (ℓ=*2*) Legendre function. In order to get exactly the (ℓ=*2*) Legendre function in (23.3.7) it is necessary to insert a factor of *-1/2*.

$$V^{quadrupole}(r) = -\frac{1}{2}\frac{\partial}{\partial z}V^{dipole}(r) = -\frac{1}{2}\frac{\partial}{\partial z}\frac{qz}{r^3} = q\frac{3z^2-r^2}{2r^5} = \frac{qP_2(\cos\theta)}{r^3} \qquad (23.3.13)$$

Similarly the (ℓ=*3*) *octupole* function is *-1/3* of a *z*-derivative of the quadrupole potential.

$$V^{octupole}(r) = \frac{-1}{3}\frac{\partial}{\partial z}V^{quadrupole}(r) = \frac{-1}{3}\frac{\partial}{\partial z}\frac{3z^2-r^2}{2r^5} = q\frac{5z^3-3z}{2r^5} = \frac{qP_3(\cos\theta)}{r^4} \qquad (23.3.14)$$

The copy-with-sign-change-and-displace process can be continued indefinitely and each time the number of monopoles doubles as shown in Fig. 23.3.4. After ℓ derivatives by *z* there are 2^ℓ poles. The resulting field is the general *linear multi-pole* or *2^ℓ-pole potential* field.

$$V^{2^\ell-pole}(r) = \frac{(-1)^\ell}{\ell!}\frac{\partial^\ell}{\partial z^\ell}\left(\frac{q}{r}\right) = \frac{qP_\ell(\cos\theta)}{r^{\ell+1}} \qquad (23.3.15)$$

More reasons for the extra factors $(-1)^\ell$ and $1/\ell!$ are seen later. The resulting discrete charge distributions are shown in the upper portion of Fig. 23.3.4. Each distribution for ℓ = *1, 2, 3, 4, 5,..* is made of charges equal to *q* times the binomial coefficients $C^\ell_n = \ell!/(\ell-n)!n!$ with alternating signs such as occur in the Pascal array (3.1.25) for discrete derivative representations.

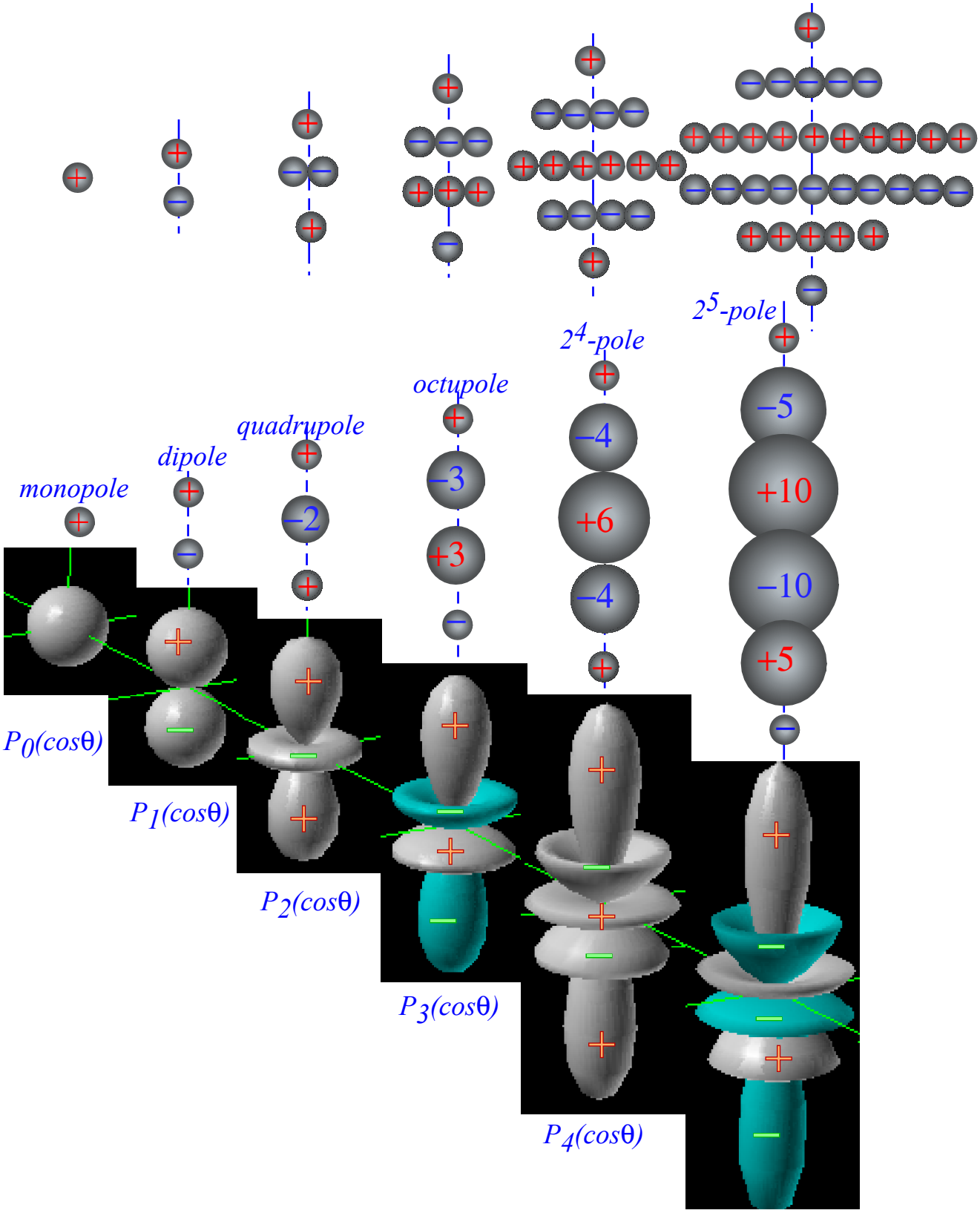

Fig. 23.3.4 Linear 2^k-pole charge arrays and potential or wave function plots.

A list the first five $P_\ell\,(cos\theta)$ functions which are plotted in the lower part of Fig. 23.3.4 is here.

$$P_0(z)=1\ , \qquad P_1(z)=z\ ,$$
$$P_2(z)=\frac{1}{2}\left(3z^2-1\right)\ , \qquad P_3(z)=\frac{1}{2}\left(5z^3-3z\right)\ , \qquad (23.3.15)_{\text{examples}}$$
$$P_4(z)=\frac{1}{8}\left(35z^4-30z^2+3\right)\ , \qquad P_5(z)=\frac{1}{8}\left(63z^5-70z^3+15z\right)\ ,$$

The node structure of the $P_\ell\,(cos\theta)$ functions reflects the discrete point sources used to define them. The relation between the potential function $V(r;\theta)$ and the infinitesimal linear point charge distribution which produces it is fairly easy to see. A positive or negative charge contributes a concentric positive or negative potential sphere around it. Stacking the charges on top of each other flattens the spheres in the middle and elongates the spheres on the ends.

Neighboring flattened spheres have opposite sign as do their source charges. In between neighboring spheres are special polar angular directions or cones on which the potential is exactly zero. These angles are called *magic angles*. Perhaps, the best known of these is the *d-function magic angle* along which the Legendre function $P_2\,(cos\theta)$ is zero.

$$P_2\,(cos\theta) = 0 = (3\,cos^2\theta - 1)/2 \quad \text{, or:} \quad \theta_{magic} = cos^{-1}(1/\sqrt{3}) = 54.7° \qquad (23.3.16)$$

This angle happens also to be the polar angle of the main diagonal *(111)* direction of a cube. (Magic angles are not to be confused with angular momentum vector uncertainty-cone angles (23.1.11) which, for a wavefunction $P_\ell\,(cos\theta)$ having zero m, must be $90°$.)

The magic zero-potential cones are also nodal planes for the quantum mechanical wavefunctions $\Psi^\ell{}_0$. Indeed, it is remarkable consequence of *R(3)* symmetry that molecules, atoms, and nuclei have wave functions or probability amplitudes $\Psi^\ell{}_0$ that mimic perfectly the potential functions $P_\ell\,(cos\theta)$ of multipole charge distributions. Of course, the observed probability distributions $|\Psi^\ell{}_0|^2$, are squares of $P_\ell\,(cos\theta)$ so, at first sight, it might seem the physical connection is spoiled somewhat.

However, a commonly observed atomic radiation field has precisely the shape of the dipole function $P_1\,(cos\theta)$ shown in Fig. 23.1.4 . This comes about because a common atomic state mixture Ψ is that of a scalar ground state $\Psi^0{}_0$ and a vector excited state $\Psi^1{}_0$. Such a Ψ has an oscillating $\Psi^1{}_0$ - shaped charge distribution in much the same way that (4.3.5a) has an oscillating linear dipole.

$$\Psi^*\Psi(r,\theta,t)=\left(\left|\Psi^0_0(r)\right|^2+\left|\Psi^1_0(r,\theta)\right|^2+2\Psi^0_0(r)\Psi^1_0(r,\theta)\cos\left(\omega^1_0-\omega^0_0\right)t\right)/2$$

The oscillating term has precisely the angular dependence of a dipole wave $\Psi^1{}_0 = P_1\,(cos\theta)$. So will the Fourier spectral component of the resulting potential field at the transition (beat) frequency. Similarly, a tensor or quadrupole $\Psi^2{}_0$ can combine with $\Psi^0{}_0$ to give an oscillating quadrupole wave, though, as we will see later, this process is not as prevalent.

23.4 Multipole Expansions

The Legendre functions P_ℓ in (23.3.10), the $X^\ell{}_m$ in (23.3.8), and $D^\ell{}_{mn}$ functions (23.1.15) from which the P_ℓ and $X^\ell{}_m$ are derived, may be used to expand both Hamiltonian operators or potentials and their eigenstates or wavefunctions. This is a generalization of the Fourier analyses in Sec. 3.7(b) and Sec. 3.8 which use plane wave functions $D^k(r)=e^{ikr}$ to expand both the Hamiltonian potential and its wave solutions. Symmetry ireps $D^k(r)$ or $D^\ell{}_{mn}(\alpha\beta\gamma)$ define spectral decomposition of both the Hamiltonian operators and the symmetry operators from which they are made. Hence, the ever-present D-functions serve multiple duty as wavefunctions and matrices that transform the wavefunctions.

(a) Linear multipole expansions

The extra factors $(-1)^\ell$ and $1/\ell!$ in (23.1.25e) help simplify Taylor expansions. For example, consider the potential at $\mathbf{r}$ due to a charge q at an arbitrary point $\mathbf{r'}=z'\mathbf{e_z}=r'\mathbf{e_z}$ on the z-axis.

$$\frac{q}{|\mathbf{r}-\mathbf{r}'|}=\frac{q}{r}\quad -r'\frac{\partial}{\partial z}\left(\frac{q}{r}\right)\quad +\frac{(r')^2}{2!}\frac{\partial^2}{\partial z^2}\left(\frac{q}{r}\right)\quad -\frac{(r')^3}{3!}\frac{\partial^3}{\partial z^3}\left(\frac{q}{r}\right)+\cdots+\frac{(-r')^\ell}{\ell!}\frac{\partial^\ell}{\partial z^\ell}\left(\frac{q}{r}\right)\cdots$$
$$=\frac{q}{r}+\frac{qr'}{r^2}P_1(\cos\theta)+\frac{q(r')^2}{r^3}P_2(\cos\theta)+\frac{q(r')^3}{r^4}P_3(\cos\theta)+\cdots+\frac{q(r')^\ell}{r^{\ell+1}}P_\ell(\cos\theta)\cdots \tag{23.4.1a}$$

This is called a *linear multipole expansion*. It converges if the field point radius r is greater than the source point radius r'. If the source is farther away then r and r' must be switched to make a convergent series.

$$\frac{q}{|\mathbf{r}-\mathbf{r}'|}=\frac{q}{r'}+\frac{qr}{(r')^2}P_1(\cos\theta)+\frac{qr^2}{(r')^3}P_2(\cos\theta)+\frac{qr^3}{(r')^4}P_3(\cos\theta)+\cdots+\frac{qr^\ell}{(r')^{\ell+1}}P_\ell(\cos\theta)\cdots \tag{23.4.1b}$$

The potential at far-r due to an array of point charges $q_1, q_2, q_3, \ldots$ at $r'_1, r'_2, r'_3,\ldots$respectively, is

$$V_{far}(r)=\frac{Q^0_{near}}{r}+\frac{Q^1_{near}}{r^2}P_1(\cos\theta)+\frac{Q^2_{near}}{r^3}P_2(\cos\theta)+\cdots+\frac{Q^\ell_{near}}{r^{\ell+1}}P_\ell(\cos\theta)\cdots \tag{23.4.2a}$$

where *near linear multipole moments* Q^ℓ are defined for near source radii $r'_k < r$ causing far fields.

$$Q^0_{near}=\sum_k q_k\ ,\quad Q^1_{near}=\sum_k q_k r'_k\ ,\quad Q^2_{near}=\sum_k q_k r'^2_k\ ,\ldots..Q^\ell_{near}=\sum_k q_k r'^\ell_k\ \cdots \tag{23.4.2b}$$

For far sources at large radii $r'_k > r$ the second type of expansion is needed to have convergence.

$$V_{near}(r)=Q^0_{far}+Q^1_{far}\,r\,P_1(\cos\theta)+Q^2_{far}\,r^2P_2(\cos\theta)+\cdots+Q^\ell_{far}\,r^\ell P_\ell(\cos\theta)\cdots \tag{23.4.2c}$$

where *far linear multipole moments* Q^ℓ are defined for far source radii $r'_k > r$ causing near fields.

$$Q^0_{far}=\sum_k\frac{q_k}{r'_k}\ ,\quad Q^1_{far}=\sum_k\frac{q_k}{r'^2_k}\ ,\quad Q^2_{far}=\sum_k\frac{q_k}{r'^3_k}\ ,\quad .....Q^\ell_{far}=\sum_k\frac{q_k}{r'^{\ell+1}_k}\ \cdots \tag{23.4.2d}$$

Far-linear charge distributions are confined to the far z-axis. They are undefined or ambiguous for source radii that are zero or negative. Now we discuss the full three-dimensional theory that resolves sign ambiguity and works for practically any array of charges, near and far. It uses full $Y^l{}_m$ functions.

(b) The addition (multiplication) theorem

Legendre polynomial terms $r^\ell P_\ell\,(\cos\theta)$ or $(1/r^{\ell+1})P_\ell\,(\cos\theta)$ are fine for expanding a potential V due to charges that are all lined up on the z-axis. Such a V has azimuthal-rotational $R_z(2)$-symmetry and is a function $V(r,\theta)$ only of radius r and polar angle θ. But, a potential due to a charge at an arbitrary position (r,α,β) requires a more general expansion in terms of spherical harmonic $Y^\ell_m(\phi,\theta)$-functions (23.1.16) or multipole $X^\ell_m(\phi,\theta)$-functions (23.1.22) which have the necessary dependence on an azimuthal angle ϕ.

Euler symmetry rotations $\mathbf{R}(\alpha,\beta,\gamma)$ are very helpful for rotating on-z-axis charge points in angular position state $|0,0,0\rangle$ to an arbitrary off-axis position state $|\alpha,\beta,0\rangle$. We use (23.1.19a)

$$\mathbf{R}(\alpha,\beta,0)\,|0,0,0\rangle = |\alpha,\beta,0\rangle$$

The third Euler "twist" angle γ can be ignored since a point charge has "smooth" internal azimuthal symmetry and no definable body orientation to twist about its radial axis. The same operator $\mathbf{R}(\alpha,\beta,0)$ may be applied to any state of azimuthal symmetry including an $(m=0)$-angular momentum state $\left|{}^{\ell}_{0}\right\rangle$ with a Legendre $P_\ell\,(\cos\theta)$ wavefunction. Lab transform rule (23.1.20a) is used with harmonic definition (23.1.16).

$$\left|{}^{\ell}_{0}\right\rangle_{(\alpha,\beta)} \equiv \mathbf{R}(\alpha,\beta,0)\left|{}^{\ell}_{0,0}\right\rangle = \sum_{m=-\ell}^{\ell}\left|{}^{\ell}_{m,0}\right\rangle D^\ell_{m,0}(\alpha,\beta,0) = \sum_{m=-\ell}^{\ell}\left|{}^{\ell}_{m,0}\right\rangle Y^{\ell*}_m(\alpha,\beta)\sqrt{\frac{4\pi}{2\ell+1}} \qquad (23.4.4a)$$

The amplitude at polar position state $|\phi,\theta,0\rangle$ for rotated Legendre $\left|{}^{\ell}_{0}\right\rangle_{(\alpha,\beta)}$ state is their bra-ket product.

$$\begin{aligned}\left\langle\phi,\theta\right|{}^{\ell}_{0}\Big\rangle_{(\alpha,\beta)} &= \left\langle\phi,\theta\right|\mathbf{R}(\alpha,\beta,0)\left|{}^{\ell}_{0,0}\right\rangle \\ &= \sum_{m=-\ell}^{\ell}\left\langle\phi,\theta\right|{}^{\ell}_{m,0}\Big\rangle Y^{\ell*}_m(\alpha,\beta)\sqrt{\frac{4\pi}{2\ell+1}} \\ &= \sum_{m=-\ell}^{\ell} Y^\ell_m(\phi,\theta)Y^{\ell*}_m(\alpha,\beta)\frac{4\pi}{2\ell+1}\end{aligned} \qquad (23.4.4b)$$

As seen in Fig. 23.4.1, a rotated Legendre state is still symmetric about its new $z(\alpha,\beta)$ axis, and so the amplitude (23.4.4b) must equal $P_\ell\,(\cos\Theta)$ with Θ being the angle between axes $z(\phi,\theta)$ and $z(\alpha,\beta)$.

$$P_\ell(\cos\Theta) = \sum_{m=-\ell}^{\ell} Y^\ell_m(\phi,\theta)Y^{\ell*}_m(\alpha,\beta)\frac{4\pi}{2\ell+1} \qquad (23.4.5a)$$

This relation is known as the *harmonic addition theorem*. It could also be called the *multiplication* theorem since it is the $(0,0)$ component of a representation of a group product $\mathbf{R}^\dagger(\alpha,\beta,0)\mathbf{R}(\phi,\theta,0) = \mathbf{R}(\Phi,\Theta,0)$.

$$\begin{aligned}{}_{(\alpha,\beta)}\left\langle{}^{\ell}_{0}\right|{}^{\ell}_{0}\Big\rangle_{(\phi,\theta)} &= \left\langle{}^{\ell}_{0}\right|\mathbf{R}^\dagger(\alpha,\beta,0)\mathbf{R}(\phi,\theta,0)\left|{}^{\ell}_{0}\right\rangle = \left\langle{}^{\ell}_{0}\right|\mathbf{R}(\Phi,\Theta,0)\left|{}^{\ell}_{0}\right\rangle \\ &= \sum_{m=-\ell}^{\ell} D^{\ell\dagger}_{0,m}(\alpha,\beta,0)D^\ell_{m,0}(\phi,\theta,0) = D^\ell_{0,0}(\Phi,\Theta,0) = P_\ell(\cos\Theta)\end{aligned} \qquad (23.4.5b)$$

We will show that the Euler angles of operator $\mathbf{R}(\Phi,\Theta,0)$ are the polar angles $\alpha=\Phi$ and $\beta=\Theta$ of the $z(\phi,\theta)$ axis in the $(\alpha\beta)$-tipped "body-frame" that has the Legendre function on its $z(\alpha,\beta)$ axis. (See Fig. 23.4.1.) Indeed, the $P_3\,(\cos\theta)$ function, which happens to be the example used in Fig. 23.4.1, could be a wavefunction of a rotating diatomic molecule, or an electronic f-orbital, or some other object with total angular momentum $\ell=3$. Or, it could represent the potential of charge array with an octupole moment. In any case, the $z(\alpha,\beta)$ axis can be regarded as a "body-axis" of something with azimuthal symmetry, and, because of that symmetry, no component of angular momentum along its body axis.

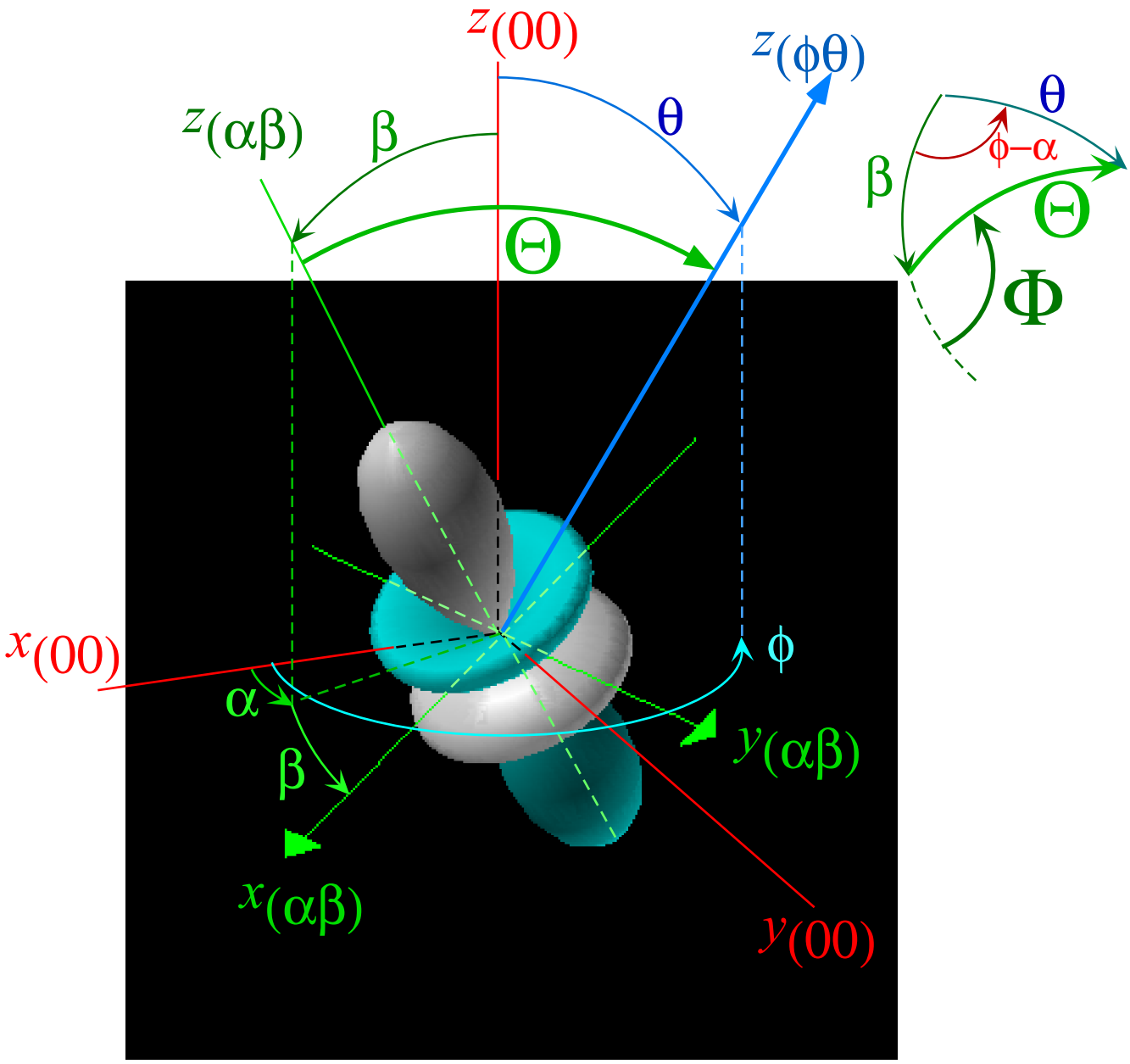

Fig. 23.4.1 Coordinate geometry of (α,β) tipped Legendre function and arbitrary field point z(ϕ,θ).

A *p*-wavefunction ($\ell=1$:$P_1(\cos\theta)=\cos\theta$) has the simple symmetry of a unit-vector. It, too, can be pointed in the $z(\alpha,\beta)$ direction of Fig. 23.4.1 by combining the *x*, *y*, and *z* waves shown in Fig. 23.3.1.
For $(\ell=1)$, (23.4.5b) is the *(z,z)-direction cosine* in the vector irep (23.3.5a). Vectors $|z\rangle_{(\alpha,\beta)}$ and $|z\rangle_{(\phi,\theta)}$ are polar-angular forms residing in the (third) *z*-column of (23.3.5a) with the following dot-product.

$$ {}_{(\alpha,\beta)}\left\langle \begin{matrix}1\\0\end{matrix}\middle|\begin{matrix}1\\0\end{matrix}\right\rangle_{(\phi,\theta)} = \begin{pmatrix}\cos\alpha\sin\beta & \sin\alpha\sin\beta & \cos\beta\end{pmatrix}\bullet\begin{pmatrix}\cos\phi\sin\theta\\ \sin\phi\sin\theta\\ \cos\theta\end{pmatrix} \qquad (23.4.5c) $$

$$ =_{(\alpha,\beta)}\left\langle \begin{matrix}1\\z\end{matrix}\middle|\begin{matrix}1\\z\end{matrix}\right\rangle_{(\phi,\theta)} = \cos(\phi-\alpha)\sin\theta\sin\beta+\cos\theta\cos\beta = P_1(\cos\Theta) = \cos\Theta $$

The last line is an ancient *spherical triangular cosine law* relating the cosine of the great-circle arc Θ to its adjacent θ and β arcs and opposite angle $(\phi-\alpha)$ as sketched in the upper portion of Fig. 23.4.1.

It is important to understand the matrix multiplication (23.4.5b-c) geometrically. The operations

$$\mathbf{R}(\Phi,\Theta,0)\,|z\rangle_{(0,0)} = \mathbf{R}^\dagger(\alpha,\beta,0)\mathbf{R}(\phi,\theta,0)\,|z\rangle_{(0,0)} \qquad (23.4.5d)$$
$$|z\rangle_{(\Phi,\Theta)} = \mathbf{R}^\dagger(\alpha,\beta,0)\,|z\rangle_{(\phi,\theta)}\ ,$$

say, "R$(\Phi,\Theta,0)$-rotating lab $|z\rangle_{(0,0)}$-axis over to $|z\rangle_{(\Phi,\Theta)}$ axis is the same as $\mathbf{R}(\phi,\theta,0)$-rotating the lab $|z\rangle_{(0,0)}$-axis over to the $|z\rangle_{(\phi,\theta)}$-axis and then undoing the body $|z\rangle_{(\alpha,\beta)}$-axes tipping using $\mathbf{R}^\dagger(\alpha,\beta,0)$."

In other words, polar angles for the $|z\rangle_{(\phi,\theta)}$-axis in the body frame are (Φ,Θ) and in the lab frame, too, if you $\mathbf{R}^\dagger(\alpha,\beta,0)$-rotate body frame and $|z\rangle_{(\phi,\theta)}$ back to the lab. So, the body frame polar azimuth Φ and Θ are found from *y*-and-*z*-components in the *z*-column of the $\mathbf{R}^\dagger(\alpha,\beta,0)\mathbf{R}(\phi,\theta,0)$ product matrix.

$$\begin{pmatrix} \cos\alpha\cos\beta & \sin\alpha\cos\beta & -\sin\beta \\ -\sin\alpha & +\cos\alpha & 0 \\ \cos\alpha\sin\beta & \sin\alpha\sin\beta & \cos\beta \end{pmatrix}\cdot\begin{pmatrix} \cos\phi\cos\theta & -\sin\phi & \cos\phi\sin\theta \\ \sin\phi\cos\theta & +\cos\phi & \sin\phi\sin\theta \\ -\sin\theta & 0 & \cos\theta \end{pmatrix}=\begin{pmatrix} \cdot & \cdot & \cos\Phi\sin\Theta \\ \cdot & \cdot & \sin\Phi\sin\Theta \\ \cdot & \cdot & \cos\Theta \end{pmatrix}$$

(23.4.5e)

$$=\begin{pmatrix} \cdot & \cdot & \cos\alpha\cos\beta\cos\phi\sin\theta+\sin\alpha\cos\beta\sin\phi\sin\theta-\sin\beta\cos\theta \\ \cdot & \cdot & -\sin\alpha\cos\phi\sin\theta+\cos\alpha\sin\phi\sin\theta \\ \cdot & \cdot & \cos\alpha\sin\beta\cos\phi\sin\theta+\sin\alpha\sin\beta\sin\phi\sin\theta+\cos\beta\cos\theta \end{pmatrix}=\begin{pmatrix} \cdot & \cdot & \cos(\phi-\alpha)\cos\beta\sin\theta-\sin\beta\cos\theta \\ \cdot & \cdot & \sin(\phi-\alpha)\sin\theta \\ \cdot & \cdot & \cos(\phi-\alpha)\sin\beta\sin\theta+\cos\beta\cos\theta \end{pmatrix}$$

A determining Φ equation results that is a *spherical triangular sine law* for arcs in Fig. 23.1.8.

$$\sin\Phi\,\sin\Theta = \sin(\phi-\alpha)\,\sin\theta \quad \text{or:}\quad \sin\Phi\,/\,\sin(\phi-\alpha) = \sin\theta\,/\,\sin\Theta \qquad (23.4.5f)$$

It equates the ratios *sin(arc) / sin(opposite angle)* for a spherical triangle sketched in Fig. 23.1.8.

Finally, consider the (α,β)-tipped equivalent **S** of $\mathbf{R}(\Phi,\Theta,0)$ defined as follows.

$$\mathbf{S} = \mathbf{R}(\alpha,\beta,0)\ \mathbf{R}(\Phi,\Theta,0)\ \mathbf{R}^\dagger(\alpha,\beta,0) \qquad (23.4.6)$$

S does the same rotation of the "body" axis $z(\alpha,\beta)$ to the field point axis $z(\phi,\theta)$ that $\mathbf{R}(\Phi,\Theta,0)$ did to rotate the lab axis $z(0,0)$ to the equivalent field point axis $z(\Phi,\Theta)$. **S** is $\mathbf{R}(\Phi,\Theta,0)$ with switched factors.

$$\mathbf{S} = \mathbf{R}(\alpha,\beta,0)\ \mathbf{R}^\dagger(\alpha,\beta,0)\mathbf{R}(\phi,\theta,0)\ \mathbf{R}^\dagger(\alpha,\beta,0) = \mathbf{R}(\phi,\theta,0)\ \mathbf{R}^\dagger(\alpha,\beta,0) \qquad (23.4.7a)$$
$$= \mathbf{R}(\phi,0,0)\ \mathbf{R}(0,\theta-\beta,0)\ \mathbf{R}(-\alpha,0,0) = \mathbf{R}(\phi,\theta-\beta,-\alpha) \qquad (23.4.7b)$$

This switched rotation reduces to an Euler form $\mathbf{S}=\mathbf{R}(\phi,\theta-\beta,-\alpha)$ which is a simpler function of angles $(\alpha,\beta,\phi,\theta)$ than the original rotation $\mathbf{R}(\Phi,\Theta,0)$ given by (23.4.5d). You should verify the effect of $\mathbf{S}=\mathbf{R}(\phi,\theta-\beta,-\alpha)$ on $z(\alpha,\beta)$: first a *z*-rotation by -α, y-rotation by θ–β, and finally a *z*-rotation by φ. Use Fig. 23.4.1 to help follow the Euler chain of operations that rotate "body" axis $z(\alpha,\beta)$ to the field point $z(\phi,\theta)$.

It is easy to show that $\mathbf{S}=\mathbf{R}(\phi,\theta-\beta,-\alpha)$ rotates vector axes $z(\alpha,\beta)$ into $z(\phi,\theta)$ axes as follows.

$$|z\rangle_{(\phi,\theta)} = \mathbf{S}|z\rangle_{(\alpha,\beta)} = \mathbf{R}(\phi,\theta,0)\mathbf{R}^\dagger(\alpha,\beta,0)|z\rangle_{(\alpha,\beta)} = \mathbf{R}(\phi,\theta,0)|z\rangle_{(0,0)}\ , \qquad (23.4.8a)$$

It does the same for linear multipole states, potentials, or waves of arbitrary $\ell = 1,2$, that sit on these axes.

$$\left|\begin{smallmatrix}\ell\\0\end{smallmatrix}\right\rangle_{(\phi,\theta)} = \mathbf{S}\left|\begin{smallmatrix}\ell\\0\end{smallmatrix}\right\rangle_{(\alpha,\beta)} = \mathbf{R}(\phi,\theta,0)\mathbf{R}^\dagger(\alpha,\beta,0)\left|\begin{smallmatrix}\ell\\0\end{smallmatrix}\right\rangle_{(\alpha,\beta)} = \mathbf{R}(\phi,\theta,0)\left|\begin{smallmatrix}\ell\\0\end{smallmatrix}\right\rangle_{(0,0)} \qquad (23.4.8b)$$

(c) 3-Dimensional multipole expansions

Linear multiple expansions such as (23.4.1) may be upgraded to 3-dimensional ones by using the addition theorem (23.4.5). A single point charge q_1 located on an arbitrary "body" axis at $\mathbf{r}_1 = (r_1, \phi_1, \theta_1)$ is expanded as follows according to whether the charge radius r_1 is near $(r_1 < r)$ or far $(r_1 > r)$.

$$\frac{q_1}{|\mathbf{r}-\mathbf{r}_1|} = \begin{cases} \sum_{\ell=0} \frac{q_1 r_1^{\ell}}{r^{\ell+1}} P_\ell(\cos\Theta_1) = \sum_{\ell=0} \sum_{m=-\ell}^{\ell} \frac{4\pi q_1 r_1^{\ell}}{(2\ell+1) r^{\ell+1}} Y_m^{\ell *}(\phi_1,\theta_1) Y_m^{\ell}(\phi,\theta) & \text{for: } r > r_1 \\ \sum_{\ell=0} \frac{q_1 r^{\ell}}{r_1^{\ell+1}} P_\ell(\cos\Theta_1) = \sum_{\ell=0} \sum_{m=-\ell}^{\ell} \frac{4\pi q_1 r^{\ell}}{(2\ell+1) r_1^{\ell+1}} Y_m^{\ell *}(\phi_1,\theta_1) Y_m^{\ell}(\phi,\theta) & \text{for: } r < r_1 \end{cases} \tag{23.4.9}$$

For an array of charges $q_1, q_2,$ ... at (r_1, ϕ_1, θ_1), (r_2, ϕ_2, θ_2) ,....the potential expands into two series, one for "near" charges and one for "far" charges. It is assumed that all radii r and r_c are positive.

$$V(r,\phi,\theta) = \sum_c \frac{q_c}{|\mathbf{r}-\mathbf{r}_c|} = \begin{cases} \sum_{\ell=0} \sum_{m=-\ell}^{\ell} \frac{Q_m^{\ell}(near)}{r^{\ell+1}} Y_m^{\ell}(\phi,\theta) & \text{for: } r > r_C \\ \sum_{\ell=0} \sum_{m=-\ell}^{\ell} Q_m^{\ell}(far)\, r^{\ell}\, Y_m^{\ell}(\phi,\theta) & \text{for: } r < r_C \end{cases} \tag{23.4.10a}$$

Here the *spherical coordinate multipole moments* Q^l_m of the charge array are as follows.

$$\begin{aligned} Q_m^{\ell}(near) &= \frac{4\pi}{(2\ell+1)} \sum_{charges\ c} q_c\, r_c^{\ell}\, Y_m^{\ell *}(\phi_c,\theta_c) \qquad (for\ near\ r_c < r) \\ Q_m^{\ell}(far) &= \frac{4\pi}{(2\ell+1)} \sum_{charges\ c} \frac{q_c}{r_c^{\ell+1}}\, Y_m^{\ell *}(\phi_c,\theta_c) \qquad (for\ far\ r_c > r) \end{aligned} \tag{23.4.10b}$$

Moments of a continuous charge distribution $\rho(r, \phi, \theta)$ are summed by spherical volume integrals.

$$\begin{aligned} Q_m^{\ell}(near) &= \frac{1}{(2\ell+1)} \int_0^{2\pi} d\phi \int_0^{\pi} d\theta \sin\theta \rho(r,\phi,\theta)\, r^{\ell}\, Y_m^{\ell *}(\phi,\theta) \qquad (for\ near\ r_c < r) \\ Q_m^{\ell}(far) &= \frac{1}{(2\ell+1)} \int_0^{2\pi} d\phi \int_0^{\pi} d\theta \sin\theta \frac{\rho(r,\phi,\theta)}{r^{\ell+1}}\, Y_m^{\ell *}(\phi,\theta) \qquad (for\ far\ r_c > r) \end{aligned} \tag{23.4.10c}$$

The zeroth-moments are simply $\sqrt{4\pi}$ times the total near-charge or the total potential for far-charge.

$$Q_0^0(near) = \sqrt{4\pi} \sum_{\substack{near(r_c<r) \\ charges\ c}} q_c \quad , \qquad Q_0^0(far) = \sqrt{4\pi} \sum_{\substack{far(r_c>r) \\ charges\ c}} \frac{q_c}{r_c} \tag{23.4.10d}$$

The total zeroth-order potential is the limiting value of $V(r)$ as r approaches the origin $r=0$ and all charges (except the one precisely at $r=0$) are reclassified as far-charges.

$$V^{\substack{zeroth \\ approx.}}(r,\phi,\theta) = \frac{Q_0^0(near)}{r\sqrt{4\pi}} + \frac{Q_0^0(far)}{\sqrt{4\pi}} = \sum_{\substack{near(r_c<r) \\ charges\ c}} \frac{q_c}{r} + \sum_{\substack{far(r_c>r) \\ charges\ c}} \frac{q_c}{r_c} \cong \sum_c \frac{q_c}{|\mathbf{r}-\mathbf{r}_c|} \tag{23.4.10e}$$

The factors $\sqrt{4\pi}$ can be annoying. They result from a century-old convention of hanging the square root of a normalization factor on each wavefunction instead of putting it under the integral (or discrete sum) where it belongs. For wavefunctions $\Psi(h)$ defined by group representations $D^*(h)$, as in (23.1.16) or (23.2.4b), this old convention looks silly. The D-normalization is determined by the matrix multiplication rules ($D(g)\cdot D(h) = D(gh)$) or by projector idempotency (**P·P=P**) as first seen in (3.1.10) through (3.1.15). You cannot "hang" extra factors on

D-functions or projectors. Such factors that arise from a particular coordinate integration, summing, or counting procedure, such as (23.1.17), should be attached to that procedure, particularly in the case of a Wigner-Weyl group summation as in (23.2.4a).

Example: "Tripole" array

Calculation of multipole moments for a near-localized fixed charge distribution is made easier by using symmetry. For example, consider an array of three charges such as those shown in Fig. 23.4.2. The field has at least C_3 symmetry, actually, a full D_3 trigonal symmetry. (Recall Fig. 15.1.2.) If there were such a thing as a "tripole moment" this charge array would have it.

Recall that allowed Fourier components of a D_3 -symmetric potential must be zero-modulo-3, that is $m=0_3 = 0, \pm 3, \pm 6,...$ So, the smallest non-zero azimuthal Fourier component is $m=\pm 3$, and this means that the least multipolarity is $\ell=3$ which is a 2^3-pole or octupole moment. The only quadrupole or dipole fields that might be allowed by D_3 symmetry are ones with $m=0$, that is $X^2{}_0$ or $X^1{}_0$. Furthermore, the only octupole moment coefficients $Q^\ell{}_m$ in (23.4.10) that need to be evaluated are $Q^3{}_0$, and $Q^3{}_{\pm 3}$. For general D_3 -symmetric potentials, only. $Q^\ell{}_0$, $Q^\ell{}_{\pm 3}$, $Q^\ell{}_{\pm 6}$, ...that is, $Q^\ell{}_{0_3}$ -moments, may be non-zero.

A list of $(m=0,\pm 3)$-octupole functions derived from (23.3.8) and (23.1.15b) begins this analysis.

$$\sqrt{\frac{4\pi}{7}}r^3Y_3^3 = X_3^3 = -\frac{\sqrt{5}}{4}(x+iy)^3/4 = -\frac{\sqrt{5}}{4}r^3e^{3i\phi}\sin^3\theta \qquad (23.4.11a)$$

$$\sqrt{\frac{4\pi}{7}}r^3Y_0^3 = X_0^3 = \frac{1}{2}\left(5z^3-3zr^2\right) = \frac{1}{2}r^3\left(5\cos^3\theta-3\cos\theta\right) \qquad (23.4.11b)$$

$$\sqrt{\frac{4\pi}{7}}r^3Y_{-3}^3 = X_{-3}^3 = \frac{\sqrt{5}}{4}(x-iy)^3/4 = \frac{\sqrt{5}}{4}r^3e^{-3i\phi}\sin^3\theta \qquad (23.4.11c)$$

The far-charge case of (23.4.10b) gives the multipole moments $Q^3{}_0$, and $Q^3{}_{\pm 3}$ for Fig. 23.4.2.

$$Q_m^3(far) = \frac{4\pi}{7}\sum_{charges\ c}\frac{q_c}{r_c^4}\,Y_m^{3*}(\phi_c,\theta_c) = \sqrt{\frac{4\pi}{7}}\sum_{charges\ c}\frac{q_c}{r_c^4}\,X_m^{3*}(\phi_c,\theta_c)/r_c{}^3$$

The resulting moment coefficients are as follows.

$$\begin{aligned} Q_3^3(far) &= \sqrt{\frac{4\pi}{7}}\frac{q}{a^4}\frac{\sqrt{5}}{4}\left(e^{-3i0}+e^{-3i2\pi/3}+e^{3i2\pi/3}\right) = \sqrt{\frac{4\pi}{7}}\frac{3q\sqrt{5}}{4a^4} \\ Q_0^3(far) &= 0 \\ Q_{-3}^3(far) &= \sqrt{\frac{4\pi}{7}}\frac{3q\sqrt{5}}{4a^4} \end{aligned} \qquad (23.4.12a)$$

The resulting multipole expansion to the third order is from (23.4.10a).

$$\begin{aligned} V^{far\,q}(r,\theta,\phi) &= Q_0^0Y_0^0 + Q_3^3r^3Y_3^3 + Q_{-3}^3r^3Y_{-3}^3 = \frac{3q}{a} + \frac{3q\sqrt{5}}{4a^4}r^3e^{3i\phi} + \frac{3q\sqrt{5}}{4a^4}r^3e^{-3i\phi} \\ &= \frac{3q}{r} + \frac{3q\sqrt{5}}{2a^4}r^3\cos 3\phi + \cdots \qquad (for: r \ll a) \end{aligned} \qquad (23.4.12b)$$

If the charges are nearer the origin the expansion reverts to the following.

$$V^{near\,q}(r,\theta,\phi)=\frac{Q_0^0}{r}Y_0^0+\frac{Q_3^3}{r^4}Y_3^3+\frac{Q_{-3}^3}{r^4}Y_{-3}^3=\frac{3q}{r}+\frac{3qa^3\sqrt{5}}{4}\frac{e^{3i\phi}}{r^4}+\frac{3qa^3\sqrt{5}}{4}\frac{e^{-3i\phi}}{r^4} \qquad (23.4.12c)$$
$$=\frac{3q}{r}+\frac{3qa^3\sqrt{5}}{4}\frac{\cos 3\phi}{r^4}+\cdots \qquad (for: a<<r)$$

The angular form is a Mathieu potential discussed after (16.1.6). The resulting orbital splitting sketched in Fig. 23.4.2(b) below is discussed next.

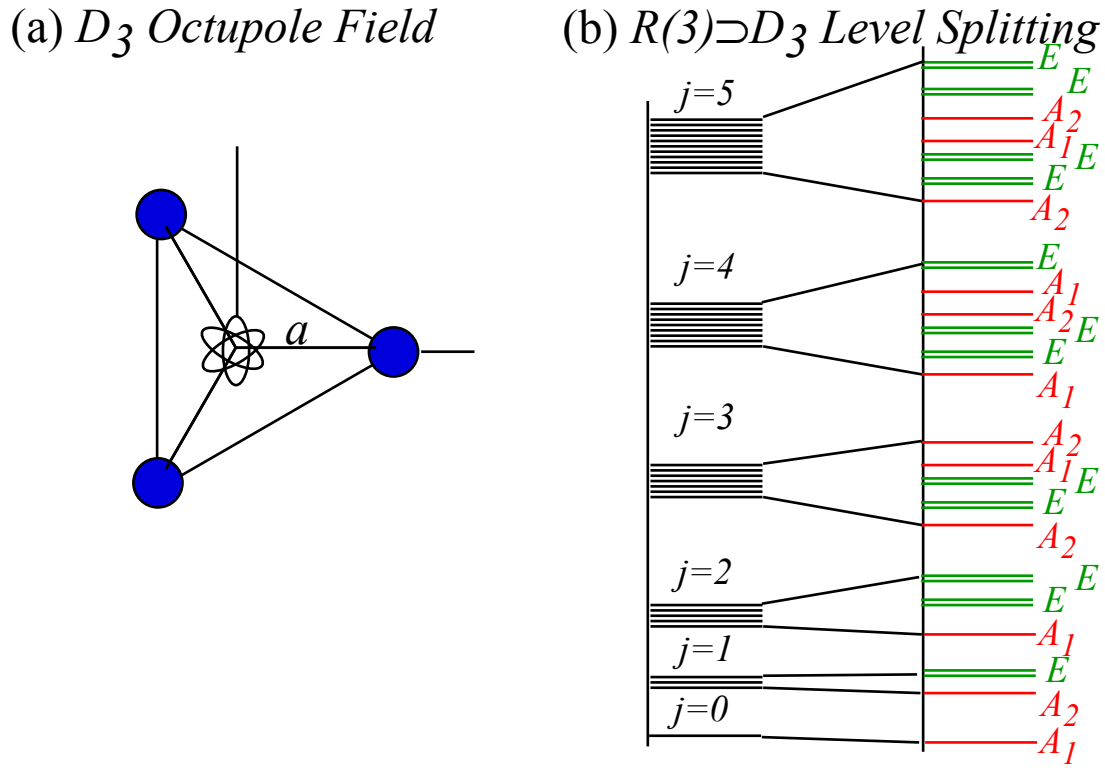

Fig. 23.4.2 Effects of D_3 symmetric field. (a) Trigonal charges around orbitals. (b) Orbital level splitting.

(d) Character analysis of orbital splitting

Putting in a triangular charge array reduces the spherical symmetry enjoyed previously by any molecule or atom occupying the space. The spherical *R(3)* symmetry has a continuum of equivalent directions and operations that are all equivalent and the atom behaves the same regardless of orientation. The presence of the charge array changes all that by reducing the symmetry to a sub-group D_3 of *R(3)* that only has six operations or equivalent positions.

Reduction of symmetry generally means lifting of degeneracy or level splitting. Higher symmetry like *R (3)* demands higher degeneracy *2j+1* for *j*-quantum levels, but lower symmetry such as D_3 is less demanding; for example D_3 never demands more than 2-fold or doublet degeneracy associated with its $E=E_1$ irreducible representations.

The $D^j_{mn}(\alpha\beta\gamma)$ matrices of (23.1.15) are, for integral $j=\ell$, *irreducible representations* of the enormous *R (3)* symmetry, that is, you cannot simultaneously block-diagonalize or reduce all $D^j_{mn}(\alpha\beta\gamma)$ matrices at once. However, you might be able to reduce or even diagonalize some subset of them, and you can certainly completely

diagonalize any *one* of them. The result of doing this would be just the matrix that represents an ω-rotation around the *z*-axis that has the following diagonal form. (Recall (23.1.15c).)

$$D^{\ell}(\omega 00)=\begin{pmatrix} e^{-i(\ell)\omega} & & & & & \\ & e^{-i(\ell-1)\omega} & & & & \\ & & e^{-i(\ell-2)\omega} & & & \\ & & & \ddots & & \\ & & & & e^{i(\ell-1)\omega} & \\ & & & & & e^{i(\ell)\omega} \end{pmatrix} \qquad (23.4.13)$$

Furthermore, it will be possible to "almost diagonalize" the D_3 sub-group of $D^{j}_{mn}(\alpha\beta\gamma)$ matrices to *1-by-1* and *2-by-2* blocks of D_3 irreducible representations, that is, something like the following.

$$D^{\ell}(D_3)=\left(\begin{array}{c|c|cc|c} D^{A_1} & & & & \\ \hline & D^{A_2} & & & \\ \hline & & D^{E}_{11} & D^{E}_{12} & \\ & & D^{E}_{21} & D^{E}_{22} & \\ \hline & & & & \ddots \\ & & & & \quad\ddots \end{array}\right) = D^{A_1}\oplus D^{A_2}\oplus\cdots\oplus D^{E}\oplus\cdots \qquad (23.4.14)$$

Each such reduction dictates the form of an ℓ-level splitting shown in Fig. 23.4.2 caused by a D_3 field. By knowing which D_3 matrices "hide" in a $D^{\ell}_{mn}(D_3)$ matrix we find the symmetry types and degeneracy of levels that will split from an ℓ-level. The exact position and ordering of the split levels is not obtained by the calculation about to be described; that comes later. However, familiarity with similar splitting in Sec. 3.5 and Sec. 3.7 provides some clues for this example.

We use trace or character analysis using D_3 characters (15.1.13) and the following trace of $D^{\ell}(\omega)$.

$$Trace D^{\ell}(\omega)= \qquad e^{-i(\ell)\omega}+e^{-i(\ell-1)\omega}+e^{-i(\ell-2)\omega}+\ldots+e^{i(\ell-1)\omega}+e^{i(\ell)\omega}$$

Deriving the sum of this geometric series is similar to spectral sums from wave optics.

$$e^{-i\omega}\ Trace D^{\ell}(\omega)=e^{-i(\ell+1)\omega}+e^{-i(\ell)\omega}+e^{-i(\ell-1)\omega}+e^{-i(\ell-2)\omega}+\ldots+e^{i(\ell-1)\omega}$$

Subtracting the preceding two equations yields a trace formula.

$$\left(1-e^{-i\omega}\right)\ Trace D^{\ell}(\omega)=-e^{-i(\ell+1)\omega}+e^{i(\ell)\omega}$$

It reduces to a familiar *sinx/x* form of an elementary diffraction function.

$$Trace D^{\ell}(\omega)=\frac{e^{-i\omega/2}\left(e^{i(\ell+1/2)\omega}-e^{-i(\ell+1/2)\omega}\right)}{e^{-i\omega/2}\left(e^{-i\omega/2}-e^{-i\omega/2}\right)}=\frac{\sin\left(\ell+\frac{1}{2}\right)\omega}{\sin\frac{\omega}{2}} \qquad (23.4.15a)$$

A geometric realization of this *sinx/x* form in Fig. 23.4.3 associates R(3) traces segments of D_n polygons.

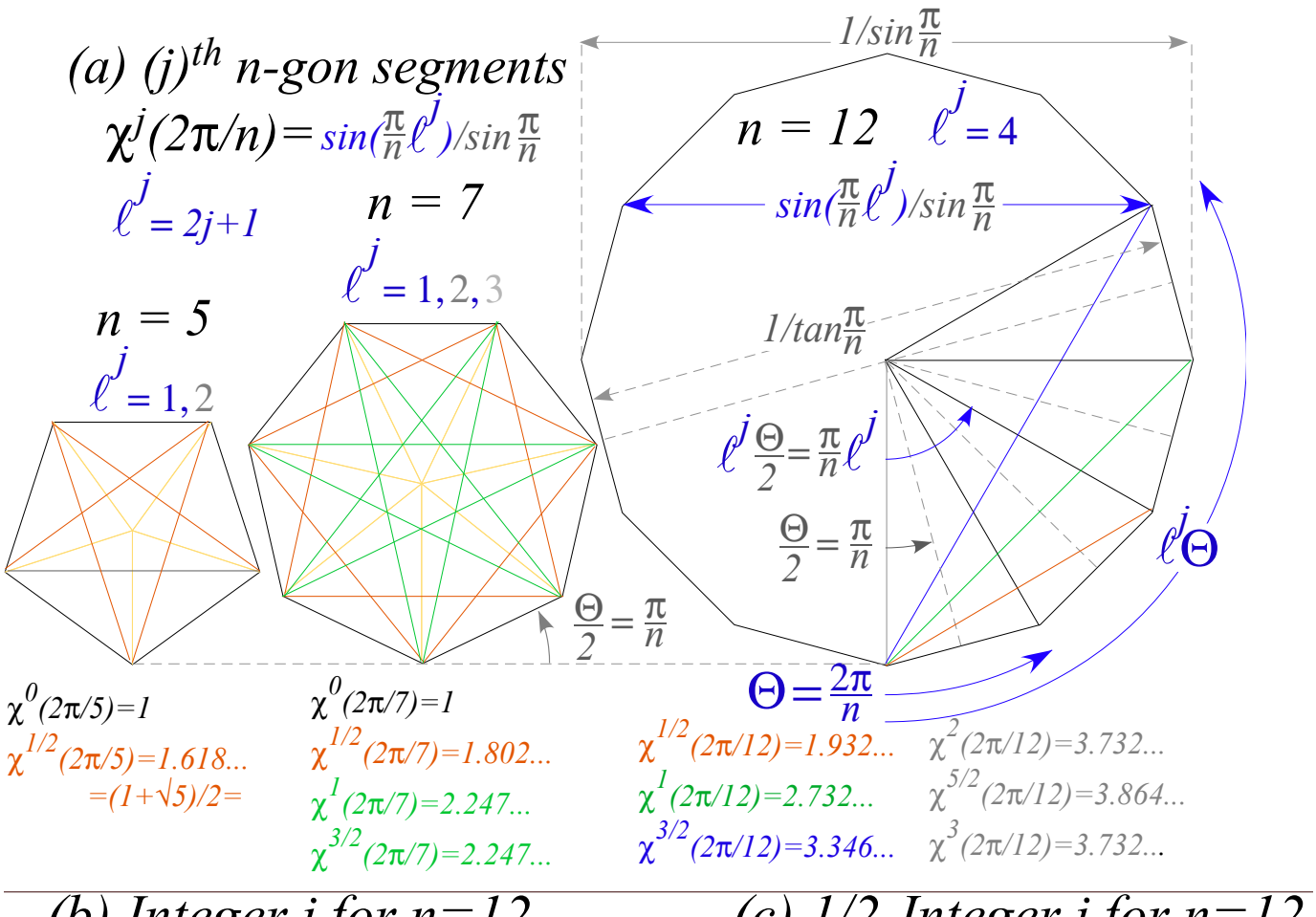

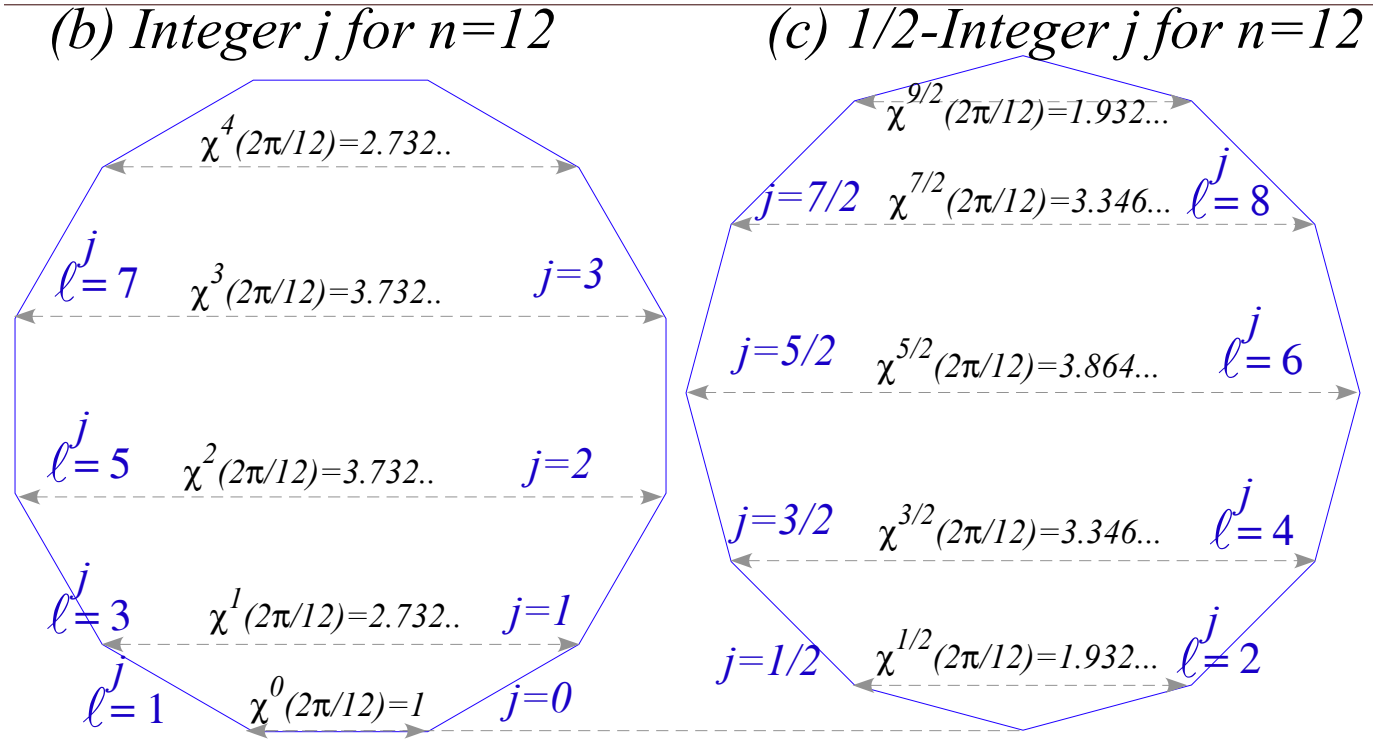

Fig. 23.4.3 Geometry of R(3)~U(2) character $\chi^j(2\pi/n)$ realized by segments of n-polygons. (a) n=5,7,12 (b-c) n=12 details for integral spin and half-integral spin

A table of *R(3)* characters for just D_3 rotations is to be compared below with D_3 characters from (15.1.13).

$$Trace D^{\ell}(\omega) = \frac{\sin(\ell + 1/2)\omega}{\sin(\omega/2)}$$

	$\omega = 0°$	$\omega = 120°$	$\omega = 180°$
$\ell = 0$	1	1	1
1	3	0	−1
2	5	−1	1
3	7	1	−1
4	9	0	1
5	11	−1	−1
6	13	1	1

$Trace D^{(\alpha)}(\omega)$ *for* D_3 *symmetry*

	$\omega = 0°$	$\omega = 120°$	$\omega = 180°$
A_1	1	1	1
A_2	1	1	−1
$E_1 = E$	2	−1	0

(23.4.15b)

From this follows the D_3 symmetry content of each *R(3)* ℓ-level splitting shown in Fig. 23.4.2.

$$\alpha - content D^{\ell}(\downarrow D_3) = f^{\alpha} = Trace D^{\ell}(\mathbb{P}^{\alpha})/\ \ell^{\alpha} \qquad = (1/{}^{\circ}D_3)\sum_{class\omega} \chi_{\omega}^{(\alpha)*} {}^{\circ} c_{\omega} Trace D^{\ell}(\omega) \qquad (23.4.15c)$$

orbital	f^{A_1}	f^{A_2}	f^{E_1}	*levels*
$\ell = 0$	1	0	0	$(s) = A_1$
1	0	1	1	$(p) = A_2 \oplus E$
2	1	2	0	$(d) = A_1 \oplus E \oplus E$
3	1	2	2	$(f) = A_2 \oplus E \oplus E \oplus A_1 \oplus A_2$
4	2	1	3	$(g) = A_1 \oplus E \oplus E \oplus A_2 \oplus A_1 \oplus E$
5	1	2	4	$(h) = A_2 \oplus E \oplus E \oplus A_1 \oplus A_2 \oplus E \oplus E$
6	3	2	4	$(i) = A_1 \oplus E \oplus E \oplus A_2 \oplus A_1 \oplus E \oplus E \oplus A_2 \oplus A_1$

(23.4.15d)

The content formula follows from analysis of class decomposition (15.2.5). The content number or "frequency" f^{α} is proportional to the reducing representation trace of all-commuting projector $\mathbb{P}^{\alpha}$. The proportionality factor is dimension ℓ^{α}, the number of 1's in each $D^{a}(\mathbb{P}^{\alpha})$. Then (15.2.5a) gives (23.4.15.c)

The $A_1EEA_2A_1EE\ A_2A_1$... pattern is a familiar one for splitting seen before in Fig. 14.2.8(a) and Fig. 15.3.3. The latter only has a single regular D_3 band cluster $A_1E(gap)\ E\ A_2(gap)$, and this what you will see repeating over and over in high orbital splitting. Deep within high D_3 barriers three levels A_1E correspond to C_3 waves 0_3 and $\pm 1_3$ that are nearly degenerate followed by gap and three more C_3 waves $E\ A_2$ of $\pm 2_3$ and a $\pm 3_3$ pair $A_2(gap)A_1$. Above the barriers the normal Bohr-like doublet sequence resumes.

$$0_3,\ \pm 1_3,\ \pm 2_3 = \pm 1_3,\ \pm 3_3 = \pm 0_3,\ \pm 4_3 = \pm 1_3,\ \pm 5_3 = \pm 1_3,\ \pm 6_3 = \pm 0_3, \ldots \qquad (23.4.16)$$

For hexagonal symmetry splitting is quite similar with added B (Brillouin "back-and-forth") representations and two kinds of doublets E_1 and E_2. Typical level splitting bands are shown in Fig. 14.2.9 and Fig. 15.5.2. Their sequence is $A_1E_1E_2B_1B_2\ E_1E_2\ A_2A_1\ E_1E_2$ … repeated.

This band cluster structure takes on more complex form in higher octahedral-cubic and icosahedral symmetries explored later on.

Problems for Chapter 23

Zeno Redux

23.1.1. A Type-*j* atomic beam sorter is capable of sorting atoms of total spin-*j* into *2j+1* separate beams, but only the top *(m=j)*-window is open. Suppose *N* of these Type-*j* analyzers are lined up to receive the preceding one's output and pass on only atoms that manage to go out its top window. The zeroth analyzer is untipped but each succeeding one is tipped by an additional π/N around the beam so that the *N-th* and final sorter is completely upside down.

(a) Give a formula for the fraction *f(j,N)* of atoms that make it all the way through. (First: What's the final state of any atom that gets through?)

(b) Give approximate *f(j,N)* for high *N* and *j* by algebraic expression $f^{\sim}(j,N)$ and evaluate numerically for *N=4* and *j=10* and for *N=4* and *j=1/2*. Check each $f^{\sim}$ against *f*.

Fundamental literal interpretations

23.1.2. If a Type-*j* analyzer is tipped by angle β (not necessarily small) and feeds its top window into a second untipped Type-*j* analyzer, the latter will sort the output into all of its *2j+1* state-*m*-counters. However, for high-*j* relatively few counters get most of the counts.

(a) Use literal interpretation of $|^{j}{}_{m}\rangle$ to derive approximate formula for number Δm of busy counters and most probable *m*-value. Test out your formula with *j=20* for β=*45°* and for β=*90°*. (May refer to Fig. *23.2.2*a-c.)

(b) If you were to add the count rates of each counter-*m* in the second analyzer multiplied by the actual value *m*, that would give an expectation value $\langle J_Z\rangle^R$ for the *z*-component J_Z of angular momentum coming out of the first β-tipped analyzer.

(a) Show that: $\langle J_Z\rangle^R = {}^R\left\langle \begin{matrix} j \\ j \end{matrix}\right| J_Z \left|\begin{matrix} j \\ j \end{matrix}\right\rangle^R$ where: $\left|\begin{matrix} j \\ m \end{matrix}\right\rangle^R = R(0\beta 0)\left|\begin{matrix} j \\ m \end{matrix}\right\rangle$

(b) Give an exact formula for $\langle J_Z\rangle^R$ in terms of *j* and β.

(Hint : First derive $R^{\dagger}(0\beta 0)\, J_Z\, R(0\beta 0) = (?)\, J_Z + (?)\, J_X$.)

(c) Give exact formula for $\langle (J_Z)^2\rangle$ in terms of *j* and β .

(d) Derive standard deviation $\Delta J_Z\,(j,\beta) = \sqrt{\langle (J_Z - \langle J_Z\rangle)^2\rangle}$ and compare to Δm in part (a).

Splat!

23.1.3. A diatomic molecule is in a *(j=2 , m=0)* eigenstate. (First, what is the body *n*-quantum number?) Suppose a quantum "fly swatter" smashes the thing onto the *XZ*-plane. Compare the probability it winds up tipped between *54.73°* and *54.74°* from the *Z*-axis to that probability for a *(j=0 , m=0)* eigenstate. (with *±1%* error)